Dear Author,

Please, note that changes made to the HTML content will be added to the article before publication, but are not reflected in this PDF.

Note also that this file should not be used for submitting corrections.

Engineering Analysis with Boundary Elements xxx (xxxx) xxx

Contents lists available at ScienceDirect

Engineering Analysis with Boundary Elements

journal homepage: www.elsevier.com/locate/enganabound

A BEM approach to the evaluation of warping functions in the Saint Venant theory

Q1 Massimo Paradiso*, Nicolò Vaiana, Salvatore Sessa, Francesco Marmo, Luciano Rosati

Department of Structures for Engineering and Architecture, University of Naples Federico II, Naples, Italy

ARTICLE INFO

Keywords:
Neumann problem
Boundary elements
Beam cross section
Shear stresses

ABSTRACT

The paper illustrates the numerical procedure, based upon a Boundary Element (BE) approach, developed to efficiently evaluate the warping functions in the Saint Venant theory of beam-like solids having both compact and thin-walled sections. Specifically, Chebyshev nodes are selected as collocation points of the BE formulation associated with the relevant pure Neumann problem and the entries of the resulting linear system of equations are evaluated analytically by invoking recursive formulas.

Assuming a polynomial interpolation for the unknown function over each boundary element, we show that a reduction in the numerical accuracy of the solution is achieved if the polynomial degree exceeds a given order strictly related to the strategy adopted to discretize the boundary. For this reason, in order to automatically cope both with compact and thin-walled domains, a general criterion has been established for properly selecting the best combination of polynomial degree and edge discretization capable of reducing the numerical error of the procedure below a given tolerance.

1. Introduction

The shear stress analysis in the Saint Venant theory of beam-like solids [1,2] and related one-dimensional (1D) models [3–9] represents a classical problem in the theory of elasticity. In particular, it has been recently proved [3] that a 1D beam model can be derived so as to ensure both energetic and kinematic consistency with the Saint Venant three-dimensional (3D) model.

Full exploitation of the new beam model requires the evaluation of additional tensors which are defined as suitable functions of the torsion and shear warping functions defined over the cross section [3].

Hence the preliminary step to the application of the beam model presented in [3] is the solution of the following harmonic problems with pure Neumann boundary conditions, in short pure Neumann problems:

$$\begin{cases} \varphi\nabla^2 = 0\,, & \forall \mathbf{r} \in \Sigma\,, \\ \varphi\nabla \cdot \mathbf{n}_\partial = -\mathbf{r}^\perp \cdot \mathbf{n}_\partial\,, & \forall \mathbf{r} \in \partial\Sigma\,, \end{cases} \tag{1}$$

$$\begin{cases} \boldsymbol{\psi}\nabla^2 = \mathbf{o}\,, & \forall \mathbf{r} \in \Sigma\,, \\ (\boldsymbol{\psi} \otimes \nabla)\mathbf{n}_\partial = -\mathbf{A}\mathbf{n}_\partial\,, & \forall \mathbf{r} \in \partial\Sigma\,, \end{cases} \tag{2}$$

related to torsion and shear, respectively.

In the previous formulas, $\Sigma \subset \mathbb{R}^2$ is an arbitrarily shaped domain and $\partial\Sigma$ its boundary, ∇ denotes the gradient and ∇^2 the two-dimensional (2D) Laplacian. Furthermore, the position vector $\mathbf{r} = [x, y]^T$ is defined in a Cartesian reference frame having the origin at the centroid G of Σ, $\mathbf{r}^\perp = [-y, x]^T$ represents its counter-clockwise rotation, $\mathbf{n}_\partial$ is the outer unit normal to $\partial\Sigma$ while $\mathbf{A}$ is the symmetric tensor defined in [10]

$$\mathbf{A} = \frac{1+\bar{\nu}}{4}(\mathbf{r} \otimes \mathbf{r}) + \frac{1-3\bar{\nu}}{8}(\mathbf{r} \cdot \mathbf{r})\mathbf{I}\,, \tag{3}$$

where $\mathbf{I}$ is the identity tensor and $\bar{\nu}$ the quantity defined by

$$\bar{\nu} = \frac{\nu}{1+\nu} \tag{4}$$

as a function of the Poisson's ratio ν.

Problems analogous to (1) and (2) are encountered in linear elasticity [11], beam theory [12–15], biomechanics of brain [16] and spine [17], mechanics of planetary bodies [18], convective heat transfer [19,20].

Analytical solution of the warping functions required in the Saint Venant flexure-torsion problem are possible only for very simple domains (circle, rectangle) by using Fourier series [1,2] or conformal mapping [21].

In more complex cases numerical methods, such as the Complex Polynomial Method [22,23], the Complex Variable Boundary Element Method [24–26], the Line Element-Less Method [7,27,28], the Finite Element Method [11,29–31] and the Boundary Element Method [32–34], need to be resorted to.

* Corresponding author.
E-mail addresses: massimo.paradiso@unina.it (M. Paradiso), nicolo.vaiana@unina.it (N. Vaiana), salvatore.sessa2@unina.it (S. Sessa), f.marmo@unina.it (F. Marmo), rosati@unina.it (L. Rosati).

https://doi.org/10.1016/j.enganabound.2020.01.004
Received 6 June 2019; Received in revised form 4 December 2019; Accepted 6 January 2020
Available online xxx
0955-7997/

Please cite this article as: M. Paradiso, N. Vaiana and S. Sessa et al., A BEM approach to the evaluation of warping functions in the Saint Venant theory, Engineering Analysis with Boundary Elements, https://doi.org/10.1016/j.enganabound.2020.01.004

With specific reference to torsion problems a thorough comparison between the first three methods has been carried out in [35], although it is undoubted that the most general approaches to the evaluation of the warping functions are still represented by the FEM and the BEM.

It is well known that the FEM requires the whole domain to be discretized into two-dimensional elements (triangular or quadrilateral) so that generation and inspection of the finite element mesh can be laborious and time consuming, especially if the geometry of the domain is not simple and/or is thin-walled. In particular mesh refinement and high element density is required at critical regions of the domain such as holes, notches or corners. Moreover, while unknown fields are computed quite accurately, the evaluation of the relevant derivatives is less effective, especially in regions characterized by large gradients.

Conversely the Boundary Element Method (BEM) requires a boundary-only discretization, thus exhibiting improved accuracy on comparatively coarse meshes and reduces the number of unknowns by one order.

During the past two decades, the Boundary Element Method has rapidly improved, and is nowadays considered as a competing method to the Finite Element Method [36]. Due to its intrinsic feature about boundary discretization, the BEM has been used very successfully for domains having low perimeter/area (surface/volume) ratios. Furthermore, the method is particularly effective in computing the derivatives of the field function, e.g. stresses in solid mechanics.

This motivates the adoption of a BEM technique in solving problems (1) and (2), a strategy exploited as well for addressing torsion and flexure of composite beams [37] and solving several more refined problems related to isotropic and composite beams, see, e.g., [38] and references quoted therein.

However, a careful scoping of the literature devoted to the solution of pure Neumann problems has shown that little attention has been paid to investigate the effects that the strategy adopted to discretize the boundary and to choose the polynomial degree assumed for the unknown function has on the accuracy of the solution.

Actually, differently from the finite element approach, a finer discretization of the boundary and/or an increase of the polynomial degree over each element is not necessarily associated with a more accurate numerical solution. These aspects are particularly important for effectively addressing both compact and thin-walled sections and to investigate on the convenience of adopting constant shape functions over the boundary, a strategy usually exploited in the analysis of beam problems by BEM [33].

Moreover, the boundary element method can be affected by loss of accuracy [39] in the regions close to the boundary, a feature usually known as boundary layer effect in the BEM literature [36]. This is typically due to the possibly inaccurate evaluation of nearly singular boundary element integrals. As a matter of fact they turn out to be regular from the analytical point of view but their actual evaluation requires to handle integrals whose magnitude can be very large as the calculation point approaches the source points embedded in the boundary integral elements.

Considerable difficulties can be experienced in the evaluation of such nearly singular integrals since neither conventional Gauss quadrature rules nor the methods designed for singular integrals are applicable [40–42].

Thus, during the last two decades, a considerable effort has been devoted to develop sophisticated computational algorithms for the accurate evaluation of nearly singular integrals [43,44]. Without any claim of completeness, we mention element subdivision methods [45,46], semi-analytical methods [47–49] and the so-called nonlinear transformations [20,50–53].

In this paper we present a novel solution scheme capable of producing accurate and efficient solutions both for compact and thin-walled domains. It is obtained by collocating the boundary integral formulation that characterizes the so-called direct BEM at Chebyshev nodes, as suggested in [54], and providing an analytical evaluation of the resulting integrals based on recursive formulas. This last feature, in particular, completely by-passes the accurate evaluation of nearly singular boundary element integrals.

Compared to harmonic problems with Dirichlet boundary conditions, the Neumann problem has three peculiar features. The first one is the so-called compatibility condition that has to be fulfilled by the data assigned on the domain boundary in order to guarantee the existence of a solution.

The second one is that, to the best of the authors knowledge, no case of degenerate scale has been reported till now in the literature [55–58] for the Laplace equation with Neumann conditions.

The third and more important feature is the singular linear system of equations associated with a pure Neumann problem due to the fact that its solution is defined up to an arbitrary constant. Following the analysis developed in [59] we address this problem by adding an extra condition enforcing the vanishing of the mean value of the unknown harmonic function over the domain.

The coefficient matrix of the linear system resulting from the discretized boundary integral equation is fully populated and non-symmetric so that the efficiency in achieving a solution still represents one of the most challenging problems for the BEM [60]. Moreover, enforcement of the mean zero condition makes rectangular the augmented matrix what calls for the use of a generalized inverse in the solution of the algebraic problem associated with the continuous Neumann problem.

Adopting a polynomial expansion of the unknown function over each element we first show how the entries of the coefficient matrix and of the load vector can be evaluated analytically by means of recursive formulas proved in the paper.

A thorough numerical analysis has been carried out in order to obtain the best combination between the boundary discretization and the degree of the polynomial approximation for the harmonic function over each element. Actually, depending on the shape of the domain and the adopted discretization, the degree of the polynomial cannot be arbitrarily increased since reduction in numerical accuracy can be experienced. For this reason a suitable algorithm is proposed in order to select the optimal degree of the polynomial approximation consistent with a given discretization.

A further algorithm is illustrated in order to define the optimal combination of a discretization parameter and the polynomial degree able to provide a numerical error that is below a given tolerance independently from the shape of the beam section, either compact or thin-walled.

The paper is organized as follows. In Section 2 the numerical strategy used for the solution of a pure Neumann problem is outlined. In particular, it is shown how the differential problem is reduced to an algebraic problem requiring the evaluation of the unknown functions along the boundary. The analytical evaluation of the entries of the coefficient matrix related to the algebraic problem is addressed in Section 3 while Section 4 details the analytical expression of the known vector associated with pure Neumann problems whose solution is required for the shear stress analysis in the Saint Venant theory. In Section 5 the role of the parameters governing the boundary discretization and the interpolating functions is analyzed in detail; furthermore a criterion to control the accuracy of the numerical solution is discussed. Finally, in Section 6 the results of some numerical tests are presented for both compact and thin-walled sections, along with a comparison with analytical solutions.

2. A boundary integral solution of a pure neumann problem

In order to derive a boundary element formulation of the differential problems (1) and (2) we exploit the related weak formulation based on the second Green's identity [60]. To comprehensively address both problems, we make reference to a generic Neumann problem formulated as follows

$$\begin{cases} \Gamma\nabla^2 = 0\,, & \forall \mathbf{r} \in \Sigma\,, \\ \Gamma\nabla\cdot\mathbf{n}_\partial = \boldsymbol{\omega}\cdot\mathbf{n}_\partial\,, & \forall \mathbf{r} \in \partial\Sigma\,, \end{cases} \tag{5}$$

where $\Gamma\colon \mathbf{r}\in\Sigma\mapsto\Gamma(\mathbf{r})$ is a twice continuously differentiable scalar function and $\boldsymbol{\omega}$ defines the boundary conditions enforced on $\partial\Sigma$.

Assuming a polynomial approximation for the restriction of the harmonic function Γ to the domain boundary, an algebraic problem is assembled in order to evaluate the coefficients defining the approximated expression of the unknown function.

2.1. Weak expression of the harmonic field

The weak formulation of the differential problem (5) is derived by considering an arbitrary scalar function $\zeta(\mathbf{r})$ twice continuously differentiable on $\Sigma\subset\mathbb{R}^2$ and applying the second Green's identity [60] to get

$$\int_\Sigma \Gamma\,\zeta\nabla^2\,\mathrm{d}A - \int_{\partial\Sigma}\Gamma\,\zeta\nabla\cdot\mathbf{n}_\partial\,\mathrm{d}s = -\int_{\partial\Sigma}\zeta\boldsymbol{\omega}\cdot\mathbf{n}_\partial\,\mathrm{d}s\,. \tag{6}$$

Assuming for ζ the fundamental solution of the Laplace equation

$$\zeta = \frac{1}{2\pi}\ln\|\mathbf{r}-\mathbf{r}^*\|\,, \qquad \zeta\nabla = \frac{\mathbf{r}-\mathbf{r}^*}{2\pi\|\mathbf{r}-\mathbf{r}^*\|^2}\,. \tag{7}$$

and recalling the properties of the Dirac delta function, Eq. (6) becomes

$$\begin{aligned} c(\mathbf{r}^*)\Gamma(\mathbf{r}^*) &- \frac{1}{2\pi}\int_{\partial\Sigma}\Gamma(\mathbf{r})\frac{\mathbf{r}-\mathbf{r}^*}{\|\mathbf{r}-\mathbf{r}^*\|^2}\cdot\mathbf{n}_\partial(\mathbf{r})\,\mathrm{d}s \\ &= -\frac{1}{2\pi}\int_{\partial\Sigma}\ln\|\mathbf{r}-\mathbf{r}^*\|\boldsymbol{\omega}(\mathbf{r})\cdot\mathbf{n}_\partial(\mathbf{r})\,\mathrm{d}s\,, \end{aligned} \tag{8}$$

where the coefficient $c(\mathbf{r}^*)$ depends on whether the source point $\mathbf{r}^*$ belongs to the interior of the domain Σ, to its boundary $\partial\Sigma$ or is an external point:

$$c(\mathbf{r}^*) = \begin{cases} 1\,, & \text{if } \mathbf{r}^*\in\mathring{\Sigma}\,, \\ \dfrac{\Delta\theta}{2\pi}\,, & \text{if } \mathbf{r}^*\in\partial\Sigma\,, \\ 0\,, & \text{if } \mathbf{r}^*\notin\Sigma\,, \end{cases} \tag{9}$$

being $\Delta\theta$ the angle between the right and the left tangent to $\partial\Sigma$ in $\mathbf{r}^*$. More specifically, let $\mathbf{t}_\partial^+$ and $\mathbf{t}_\partial^-$ be the unit tangent vectors directed according to the positive and the negative orientation of $\partial\Sigma$, respectively. In doing so, $\Delta\theta$ is the angle measured in a counter-clockwise direction from $\mathbf{t}_\partial^+$ to $\mathbf{t}_\partial^-$.

It is worth being remarked that Eq. (8) represents a weak solution of the Neumann problem (5) in the sense that the value of the unknown function Γ at the point $\mathbf{r}^*$ is expressed in terms of line integrals. This way of expressing the unknown function holds true either if the point $\mathbf{r}^*$ at which Γ is evaluated belongs to the interior or to the boundary of the 2D domain Σ. Conversely, it is conventionally assumed $\Gamma(\mathbf{r}^*)=0$ if $\mathbf{r}^*$ is outside the domain, what implies condition $(9)_3$.

On the other hand, the actual applicability of (8) relies on the capability to evaluate the relevant line integrals, as well as on the major requirement of the field Γ to be known at least on the boundary $\partial\Sigma$.

These issues will be addressed in the next section by introducing appropriate hypotheses on the shape of the domain Σ and the restriction of Γ on the boundary.

2.2. Numerical approximation of the harmonic field

Let assume Σ to be a plane domain of arbitrary polygonal shape. Its boundary $\partial\Sigma$ is the union of C simple closed curves $\partial\Sigma_b$ and the b-th boundary is a polygon having n_b straight sides $\partial\Sigma_{b_j}$ of length l_{b_j}, connecting two successive vertices, V_{b_j} and $V_{b_{j+1}}$:

$$\partial\Sigma = \bigcup_{b=1}^{C}\partial\Sigma_b = \bigcup_{b=1}^{C}\bigcup_{j=1}^{n_b}\partial\Sigma_{b_j}\,. \tag{10}$$

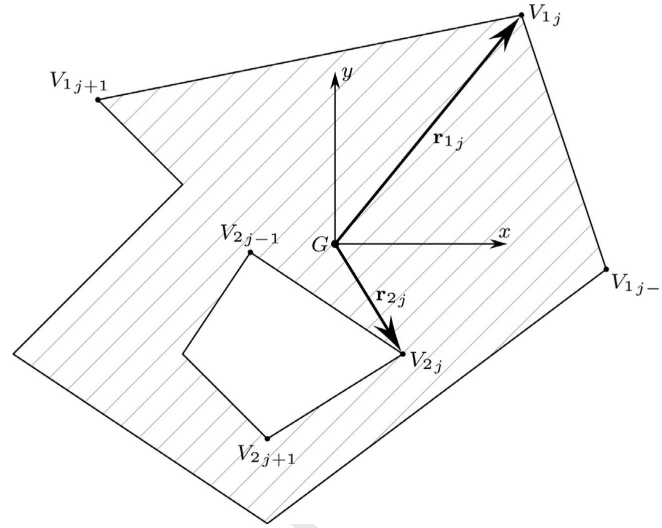

Fig. 1. Multiply-connected polygonal domain.

As shown in Fig. 1, the vertices V_{b_j} are sorted in counter-clockwise for the outer boundary $\partial\Sigma_1$ and in clockwise order for the inner boundaries $\partial\Sigma_b$, $b=2,\dots,C$. The location of the vertices in the Cartesian reference system is denoted as $\mathbf{r}_{b_j}$.

Since the domain is multiply-connected, the line integral on the section boundary $\partial\Sigma$, according to (10), can be expressed as

$$\int_{\partial\Sigma}(\cdot)\,\mathrm{d}s = \sum_{b=1}^{C}\sum_{j=1}^{n_b}\int_{\partial\Sigma_{b_j}}(\cdot)\,\mathrm{d}s_{b_j} = \sum_{k=1}^{n}\int_{\partial\Sigma_k}(\cdot)\,\mathrm{d}s_k\,, \tag{11}$$

where the pair of indices (b,j) has been replaced by $k=1,\dots,n$ in order to simplify the notation, n being the total number of segments defining the boundary:

$$n = \sum_{b=1}^{C} n_b\,.$$

Please observe that, in order to introduce a finer discretization of the boundary, it is possible to introduce a number of supplementary vertices dividing the k-th edge in m_k elements, without changing the shape of the domain. Hence the total number N of elements along the boundary is given by

$$N = \sum_{k=1}^{n} m_k\,,$$

and the line integral expressed by (11) is further modified into

$$\int_{\partial\Sigma}(\cdot)\,\mathrm{d}s = \sum_{k=1}^{n}\int_{\partial\Sigma_k}(\cdot)\,\mathrm{d}s_k = \sum_{i=1}^{N}\int_0^{l_i}(\cdot)\,\mathrm{d}s_i = \sum_{i=1}^{N}\frac{l_i}{2}\int_{-1}^{1}(\cdot)\,\mathrm{d}\mu\,, \tag{12}$$

where l_i is the length of the i-th element and the adimensional variable μ has been introduced such that

$$s_i = \frac{l_i}{2}(1+\mu)\,, \quad \mu\in[-1,1]\,. \tag{13}$$

On account of (12), Eq. (8) can be written as

$$\begin{aligned} c(\mathbf{r}^*)\Gamma(\mathbf{r}^*) &- \frac{1}{2\pi}\sum_{i=1}^{N}\frac{l_i}{2}\int_{-1}^{1}\Gamma_i(\mu)\frac{[\mathbf{r}_i(\mu)-\mathbf{r}^*]\cdot\mathbf{n}_{\partial i}}{\|\mathbf{r}_i(\mu)-\mathbf{r}^*\|^2}\,\mathrm{d}\mu \\ &= -\frac{1}{2\pi}\sum_{i=1}^{N}\frac{l_i}{2}\int_{-1}^{1}\ln\|\mathbf{r}_i(\mu)-\mathbf{r}^*\|\boldsymbol{\omega}_i(\mu)\cdot\mathbf{n}_{\partial i}\,\mathrm{d}\mu\,, \end{aligned} \tag{14}$$

where l_i is the length of the i-th boundary element.

We want to emphasize that (14) provides the value of the unknown function Γ at the arbitrary point $\mathbf{r}^*$ of the polygonal domain Σ. The assumption on the shape of the plane domain allows one to explicitly express $\mathbf{r}_i(\mu)$ as linear functions of the position vectors of the vertices.

Thus, the restriction of the harmonic field Γ to the boundary $\partial\Sigma$, represented by the functions $\Gamma_i(\mu)$, is the only unknown in (14).

In order to provide an explicit expression for the unknown functions $\Gamma_i(\mu)$, we assume a polynomial approximation by setting

$$\Gamma_i(\mu) = \sum_{p=1}^{q_i} a_p^{(i)} \mu^{p-1}, \quad \mu \in [-1, 1], \tag{15}$$

where $a_p^{(i)}$ are the q_i coefficients defining the approximating polynomial function on the i-th boundary element, μ being the adimensional local abscissa.

Assumption (15) allows one to express Eq. (14) as

$$c(\mathbf{r}^*)\Gamma(\mathbf{r}^*) - \frac{1}{2\pi}\sum_{i=1}^{N}\frac{l_i}{2}\int_{-1}^{1}\sum_{p=1}^{q_i} a_p^{(i)}\mu^{p-1}\frac{[\mathbf{r}_i(\mu)-\mathbf{r}^*]\cdot\mathbf{n}_{\partial i}}{\left\|\mathbf{r}_i(\mu)-\mathbf{r}^*\right\|^2}\,\mathrm{d}\mu = -\frac{1}{2\pi}\sum_{i=1}^{N}\frac{l_i}{2}\int_{-1}^{1}\ln\left\|\mathbf{r}_i(\mu)-\mathbf{r}^*\right\|\boldsymbol{\omega}_i(\mu)\cdot\mathbf{n}_{\partial i}\,\mathrm{d}\mu, \tag{16}$$

reducing the problem of determining N unknown functions to the one of evaluating M scalars $a_p^{(i)}$, being

$$M = \sum_{i=1}^{N} q_i. \tag{17}$$

By means of (15), the coefficients $a_p^{(i)}$ provide the unknown functions $\Gamma_i(\mu)$ along the boundary $\partial\Sigma$ and, through (16), the value of the harmonic field Γ at the point $\mathbf{r}^*$.

To evaluate the unknown coefficients, an algebraic system of M independent equations must be assembled. We will show in the next section how this purpose can be achieved by properly using expression (16).

2.3. Assembling of the algebraic system

The hypotheses introduced in the previous section have reduced the problem (5) to the one of determining the coefficients $a_p^{(i)}$, which define the restriction of Γ to the boundary $\partial\Sigma$ through the polynomial approximation (15).

A suitable number of equations can be derived from (16) by selecting M distinct source points $\mathbf{r}^*$ belonging to the boundary $\partial\Sigma$. Since for the h-th element the polynomial is defined by means of q_h coefficients, the natural choice is to consider the same number of source points by selecting q_h abscissae ξ_{h_l}:

$$\mathbf{r}^*_{h_l} = \mathbf{r}_h(\xi_{h_l}), \quad l = 1, \dots, q_h. \tag{18}$$

Eq. (16) provides the values of $\Gamma(\mathbf{r}^*_{h_l})$ at the source points (18), to be used as ordinates of the data set for the curve fitting. Hence, considering the interpolating polynomial (15) for $\Gamma_h(\xi)$ at the abscissae ξ_{h_l}, the following conditions are imposed:

$$\sum_{p=1}^{q_h} a_p^{(h)}\xi_{h_l}^{p-1} = \Gamma(\mathbf{r}^*_{h_l}) \quad l = 1, \dots, q_h. \tag{19}$$

A convenient choice of the collocation points ξ_{h_l} can be obtained by following the proposal in [54], i.e. by making reference to the Chebyshev nodes:

$$\xi_{h_l} = \cos\left(\frac{2l-1}{2q_h}\pi\right), \quad l = 1, \dots, q_h. \tag{20}$$

Such a choice also implies that the vertices of the polygons are excluded from the boundary source points $\mathbf{r}^*_{h_l}$, so that (9) provides $c(\mathbf{r}^*_{h_l}) = 1/2$.

By applying conditions (19) to the N elements of the boundary $\partial\Sigma$ and recalling the explicit expression of $\Gamma(\mathbf{r}^*_{h_l})$ through (16), the following set of M equations is obtained:

$$\frac{1}{2}\sum_{p=1}^{q_h} a_p^{(h)}\xi_{h_l}^{p-1} - \frac{1}{4\pi}\sum_{i=1}^{N} l_i\int_{-1}^{1}\sum_{p=1}^{q_i} a_p^{(i)}\mu^{p-1}\frac{[\mathbf{r}_i(\mu)-\mathbf{r}^*_{h_l}]\cdot\mathbf{n}_{\partial i}}{\left\|\mathbf{r}_i(\mu)-\mathbf{r}^*_{h_l}\right\|^2}\,\mathrm{d}\mu = -\frac{1}{8\pi}\sum_{i=1}^{N} l_i\int_{-1}^{1}\ln\left\|\mathbf{r}_i(\mu)-\mathbf{r}^*_{h_l}\right\|^2\boldsymbol{\omega}_i(\mu)\cdot\mathbf{n}_{\partial i}\,\mathrm{d}\mu, \quad l = 1, \dots, q_h, \ h = 1, \dots, N, \tag{21}$$

where, on the RHS of (21), the property

$$\ln\left\|\mathbf{r}_i(\mu)-\mathbf{r}^*_{h_l}\right\| = \frac{1}{2}\ln\left\|\mathbf{r}_i(\mu)-\mathbf{r}^*_{h_l}\right\|^2$$

has been used to simplify the evaluation of the resulting integral, see, e.g., Sections 4.1 and 4.2.

By expressing the first term in (21) as a summation respect to i through the introduction of the Kronecker delta δ_{hi}, and then grouping the LHS respect to $a_p^{(i)}$, one infers the following set of linear equations:

$$\sum_{i=1}^{N}\sum_{p=1}^{q_i}\left[4\pi\delta_{hi}\xi_{i_l}^{p-1} - 2l_i\int_{-1}^{1}\mu^{p-1}\frac{[\mathbf{r}_i(\mu)-\mathbf{r}^*_{h_l}]\cdot\mathbf{n}_{\partial i}}{\left\|\mathbf{r}_i(\mu)-\mathbf{r}^*_{h_l}\right\|^2}\,\mathrm{d}\mu\right]a_p^{(i)} = -\sum_{i=1}^{N} l_i\int_{-1}^{1}\ln\left\|\mathbf{r}_i(\mu)-\mathbf{r}^*_{h_l}\right\|^2\boldsymbol{\omega}_i(\mu)\cdot\mathbf{n}_{\partial i}\,\mathrm{d}\mu, \quad l = 1, \dots, q_h, \ h = 1, \dots, N \tag{22}$$

in the unknown parameters $a_p^{(i)}$. As usual in the direct BEM, the coefficient matrix is not symmetric.

It is important to note that the equations above are not linearly independent since the solution of the Neumann problem (5) is defined up to an arbitrary constant. Hence, the system of Eq. (22) has to be supplemented with a further condition. This is a standard caveat in BEM formulations of Neumann problem and can be addressed in several ways [60,61].

Following the analysis developed in [59], the approach herein adopted assumes that the mean value of $\Gamma(\mathbf{r})$ over the domain Σ is null:

$$\int_{\Sigma}\Gamma\,\mathrm{d}A = 0. \tag{23}$$

Condition (23) can be transformed into an algebraic equation with respect to the unknown parameters $a_p^{(i)}$ considering the equivalence (8.2) proved in the supplementary material [62]:

$$\int_{\Sigma}\left[\Gamma\mathbf{r} - \frac{1}{2}(\mathbf{r}\cdot\mathbf{r})\Gamma\nabla\right]\cdot\nabla\,\mathrm{d}A = 0;$$

actually, by applying the Divergence Theorem and recalling property $(5)_2$, one obtains

$$\int_{\partial\Sigma}\Gamma\mathbf{r}\cdot\mathbf{n}_\partial\,\mathrm{d}s = \frac{1}{2}\int_{\partial\Sigma}(\mathbf{r}\cdot\mathbf{r})\boldsymbol{\omega}\cdot\mathbf{n}_\partial\,\mathrm{d}s. \tag{24}$$

The previous two integrals are evaluated by means of (12) so that, on account of the assumption (15), one has

$$\sum_{i=1}^{N}\sum_{p=1}^{q_i}\left[l_i\int_{-1}^{1}\mu^{p-1}\mathbf{r}_i(\mu)\cdot\mathbf{n}_{\partial i}\,\mathrm{d}\mu\right]a_p^{(i)} = \frac{1}{2}\sum_{i=1}^{N} l_i\int_{-1}^{1}[\mathbf{r}_i(\mu)\cdot\mathbf{r}_i(\mu)]\boldsymbol{\omega}_i(\mu)\cdot\mathbf{n}_{\partial i}\,\mathrm{d}\mu. \tag{25}$$

Eq. (22), along with (25), provide a linear system that can be written in matrix form as

$$[\mathbf{Q}][\mathbf{a}] = [\mathbf{p}] \iff Q_{jk}a_k = b_j, \quad \begin{array}{l} j = 1, \dots, M+1, \\ k = 1, \dots, M, \end{array} \tag{26}$$

where M is the total number of scalar unknowns. Notice that the index k corresponds to the pair (i, p), while j refers to the generic equation in (22) when $j \le M$ and to (25) when $j = M+1$. Moreover being $\mathbf{Q}$ a rectangular matrix, it cannot be directly inverted, but the resolution of the linear system (26) formally requires the evaluation of the pseudo-inverse $\mathbf{Q}^+$:

$$[\mathbf{a}] = [\mathbf{Q}^+][\mathbf{p}] = \left[(\mathbf{Q}^T\mathbf{Q})^{-1}\mathbf{Q}^T\right][\mathbf{p}].$$

Observing both Eq. (22) and the additional Eq. (25), it is clear that $\mathbf{Q}$ only depends on the domain Σ, through the position of the vertices defining the polygonal boundary and the adopted discretization, as well as on the shape of the functions approximating $\Gamma_i(\mu)$ on each element. This implies that, once the classes of the interpolating functions have been fixed, the coefficient matrix $\mathbf{Q}$ for a domain Σ is uniquely determined.

On the other hand, the RHS of Eqs. (22) and (25) show that the functions $\boldsymbol{\omega}_i(\mu)$ are involved in evaluating the vector of constants $\mathbf{p}$; such functions directly derive from the boundary condition $(5)_2$ defining the specific Neumann problem.

For this reason, in the next sections we will first describe the assembling of $\mathbf{Q}$ as a general case, and then we will analyze the assembling of the vector of constants $\mathbf{p}$ with reference to the Neumann problems (1) and (2).

3. Specialization of the coefficient matrix Q and evaluation of its entries

In the previous section we have constructed $\mathbf{Q}$ as an $(M+1)\times M$ matrix. The first M rows represent the algebraic counterpart, expressed by Eq. (22), of the Neumann problem (5) and yield a square submatrix. The last row is due to the additional condition (23) expressed in the form (25).

3.1. Square submatrix of Q

To evaluate the first $M\times M$ entries of the matrix $\mathbf{Q}$, we consider the position vector $\mathbf{r}_i(\mu)$ of the generic point belonging to the i-th edge connecting the vertices $\mathbf{r}_i$ and $\mathbf{r}_{i+1}$; its expression is

$$\mathbf{r}_i(\mu) = \frac{1}{2}[(\mathbf{r}_i + \mathbf{r}_{i+1}) + \mu(\mathbf{r}_{i+1} - \mathbf{r}_i)] = \frac{1}{2}(\boldsymbol{\beta}_i + \boldsymbol{\alpha}_i\mu), \quad \mu \in [-1, 1], \tag{27}$$

where we have set

$$\boldsymbol{\alpha}_i = \mathbf{r}_{i+1} - \mathbf{r}_i, \qquad \boldsymbol{\beta}_i = \mathbf{r}_{i+1} + \mathbf{r}_i. \tag{28}$$

Moreover the outward unit normal vector can be expressed as

$$\mathbf{n}_{\partial i} = -\frac{(\mathbf{r}_{i+1} - \mathbf{r}_i)^{\perp}}{l_i} = -\frac{\boldsymbol{\alpha}_i^{\perp}}{l_i}, \tag{29}$$

so that, introducing

$$\boldsymbol{\gamma}_i^* = \frac{1}{2}\boldsymbol{\beta}_i - \mathbf{r}^*_{h_l} \tag{30}$$

and setting

$$b_i = \frac{1}{4}\boldsymbol{\alpha}_i \cdot \boldsymbol{\alpha}_i, \tag{31}$$

$$c_i^* = \boldsymbol{\alpha}_i \cdot \boldsymbol{\gamma}_i^*, \tag{32}$$

$$d_i^* = \boldsymbol{\gamma}_i^* \cdot \boldsymbol{\gamma}_i^*, \tag{33}$$

$$e_i^* = \boldsymbol{\alpha}_i \cdot \boldsymbol{\gamma}_i^{*\perp}, \tag{34}$$

one has

$$\left\|\mathbf{r}_i(\mu) - \mathbf{r}^*_{h_l}\right\|^2 = b_i\mu^2 + c_i^*\mu + d_i^*. \tag{35}$$

Hence the integral on the LHS of (22) becomes

$$2l_i\int_{-1}^{1}\mu^{p-1}\frac{[\mathbf{r}_i(\mu) - \mathbf{r}^*_{h_l}]\cdot\mathbf{n}_{\partial i}}{\left\|\mathbf{r}_i(\mu) - \mathbf{r}^*_{h_l}\right\|^2}\,\mathrm{d}\mu = 2e_i^*\int_{-1}^{1}\frac{\mu^{p-1}}{b_i\mu^2 + c_i^*\mu + d_i^*}\,\mathrm{d}\mu, \tag{36}$$

being

$$[\mathbf{r}_i(\mu) - \mathbf{r}^*_{h_l}]\cdot\mathbf{n}_{\partial i} = -\left(\boldsymbol{\gamma}_i^* + \frac{1}{2}\boldsymbol{\alpha}_i\mu\right)\cdot\frac{\boldsymbol{\alpha}_i^{\perp}}{l_i} = \frac{e_i^*}{l_i}. \tag{37}$$

Notice that in introducing the variables $\boldsymbol{\alpha}_i$, $\boldsymbol{\beta}_i$ and b_i the subscript i has been used since they refer to the i-th element, as well as the superscript * has been added for $\boldsymbol{\gamma}_i^*$, c_i^*, d_i^* and e_i^* to recall the dependence on the source point $\mathbf{r}^*_{h_l}$.

When the point $\mathbf{r}^*_{h_l}$ is collinear with $\mathbf{r}_i$ and $\mathbf{r}_{i+1}$, it turns out to be $e_i^* = 0$. Moreover the discriminant of $b_i\mu^2 + c_i^*\mu + d_i^*$ is null and the only root is

$$\bar{\mu} = -\frac{c_i^*}{2b_i} = \sqrt{\frac{d_i^*}{b_i}} = 2\frac{\left\|\boldsymbol{\gamma}_i^*\right\|}{\left\|\boldsymbol{\alpha}_i\right\|},$$

providing the abscissa such that $\mathbf{r}_i(\bar{\mu}) = \mathbf{r}^*_{h_l}$. In particular, if $|\bar{\mu}| > 1$ the source point is outside of the i-th element and the integral appearing on the RHS of (36) is well-defined. On the contrary it turns into an improper integral if $|\bar{\mu}| \le 1$, i.e. when the source point belongs to the considered element; however, it can be proved that its product with $e_i^* = 0$ always converges to 0 and the quantity expressed in (36) vanishes.

When $e_i^* \neq 0$, i.e. $\mathbf{r}^*_{h_l}$ is not collinear with $\mathbf{r}_i$ and $\mathbf{r}_{i+1}$, the discriminant of $b_i\mu^2 + c_i^*\mu + d_i^*$ turns out to be

$$c_i^{*2} - 4b_id_i^* = (\boldsymbol{\alpha}_i\cdot\boldsymbol{\gamma}_i^*)^2 - (\boldsymbol{\alpha}_i\cdot\boldsymbol{\alpha}_i)(\boldsymbol{\gamma}_i^*\cdot\boldsymbol{\gamma}_i^*) = \|\boldsymbol{\alpha}_i\|\|\boldsymbol{\gamma}_i^*\|(\cos^2\theta_i^* - 1) < 0, \tag{38}$$

being θ_i^* the angle between $\boldsymbol{\alpha}_i$ and $\boldsymbol{\gamma}_i^*$. This means that the 2-nd order polynomial has not real roots and the integral in (36) is well-defined; it can be evaluated recursively by formula (9.4) obtaining

$$2l_i\int_{-1}^{1}\mu^{p-1}\frac{[\mathbf{r}_i(\mu) - \mathbf{r}^*_{h_l}]\cdot\mathbf{n}_{\partial i}}{\left\|\mathbf{r}_i(\mu) - \mathbf{r}^*_{h_l}\right\|^2}\,\mathrm{d}\mu = 2e_i^*M_{p-1}(b_i, c_i^*, d_i^*).$$

Thus, from the LHS of (22) the element Q_{jk} assumes the form

$$4\pi\delta_{hi}\xi_{i_l}^{p-1} - 2e_i^*M_{p-1}(b_i, c_i^*, d_i^*), \tag{39}$$

in such a way that the j-th row of $\mathbf{Q}$ is obtained once the pair (h, l) is fixed while the its k-th column corresponds to the pair (i, p).

3.2. Additional row

Recalling expressions (27) and (29) of $\mathbf{r}_i(\mu)$ and $\mathbf{n}_{\partial i}$, respectively, one derives

$$\mathbf{r}_i(\mu)\cdot\mathbf{n}_{\partial i} = \frac{\lambda_i}{l_i}, \tag{40}$$

being

$$\lambda_i = \mathbf{r}_{i+1}\cdot\mathbf{r}_i^{\perp}. \tag{41}$$

Replacing (40) in the LHS of (25), the generic element of the last row of $\mathbf{Q}$ becomes

$$l_i\int_{-1}^{1}\mu^{p-1}\mathbf{r}_i(\mu)\cdot\mathbf{n}_{\partial i}\,\mathrm{d}\mu = \lambda_i\int_{-1}^{1}\mu^{p-1}\,\mathrm{d}\mu = \lambda_iP_{p-1}, \tag{42}$$

where P_{p-1} is evaluated by means of (9.2).

4. Evaluation of the known vector p

It has been noticed in Section 2.3 that the constant vector $\mathbf{p}$ of the algebraic system (22) is strictly related to the specific Neumann problem at hand, since it derives from the boundary condition in $(5)_2$.

With the aim of describing how to assemble the vector $\mathbf{p}$, it is explicitly evaluated with reference to the Neumann problems (1) and (2).

4.1. Evaluation of the vector p for the harmonic scalar field φ

Setting $\boldsymbol{\omega} = -\mathbf{r}^{\perp}$, the general problem (5) specializes to problem (1) associated with the function φ. Accordingly, the presented procedure can be used provided that the components of the vector $\mathbf{p}$ in (26) are evaluated as follows.

Let us first consider the RHS of (22), which is used to evaluate the first M elements of the column vector $\mathbf{p}$:

$$-\sum_{i=1}^{N} l_i \int_{-1}^{1} \ln \left\| \mathbf{r}_i(\mu) - \mathbf{r}_{h_l}^* \right\|^2 \boldsymbol{\omega}_i(\mu) \cdot \mathbf{n}_{\partial i} \, \mathrm{d}\mu = \sum_{i=1}^{N} l_i \int_{-1}^{1} \ln \left\| \mathbf{r}_i(\mu) - \mathbf{r}_{h_l}^* \right\|^2 \mathbf{r}_i^{\perp}(\mu) \cdot \mathbf{n}_{\partial i} \, \mathrm{d}\mu \, .$$

Vectors $\mathbf{r}_i(\mu)$ and $\mathbf{n}_{\partial i}$ have the expressions reported in (27) and (29), respectively. Thus, setting

$$f_i = \boldsymbol{\alpha}_i \cdot \boldsymbol{\beta}_i \, , \quad g_i = \boldsymbol{\alpha}_i \cdot \boldsymbol{\alpha}_i \, , \tag{43}$$

one has

$$\mathbf{r}_i^{\perp}(\mu) \cdot \mathbf{n}_{\partial i} = -\frac{1}{2 l_i}(f_i + g_i \mu) \, , \tag{44}$$

in which definitions (28) have been used. Hence, employing (35), one has

$$\sum_{i=1}^{N} l_i \int_{-1}^{1} \ln \left\| \mathbf{r}_i(\mu) - \mathbf{r}_{h_l}^* \right\|^2 \mathbf{r}_i^{\perp}(\mu) \cdot \mathbf{n}_{\partial i} \, \mathrm{d}\mu = -\frac{1}{2} \sum_{i=1}^{N} \int_{-1}^{1} \ln (b_i \mu^2 + c_i^* \mu + d_i^*)(f_i + g_i \mu) \, \mathrm{d}\mu \, .$$

As shown in Section 2.3, the discriminant of the polynomial $b_i \mu^2 + c_i^* \mu + d_i^*$ turns out $c_i^{*2} - 4 b_i d_i^* \le 0$; thus, employing formula (9.5) of the supplementary material [62] to evaluate the RHS, it is

$$-\frac{1}{2} \sum_{i=1}^{N} \int_{-1}^{1} \ln (b_i \mu^2 + c_i^* \mu + d_i^*)(f_i + g_i \mu) \, \mathrm{d}\mu = -\frac{1}{2} \sum_{i=1}^{N} \left[f_i L_0(b_i, c_i^*, d_i^*) + g_i L_1(b_i, c_i^*, d_i^*) \right] . \tag{45}$$

We recall that the superscript * refers to dependence on the source point $\mathbf{r}_{h_l}^*$ in evaluating the coefficients c_i^*, d_i^*. Thus, by suitably modifying the position of the source point, as specified in (18) and (20), the first M components of the column vector $\mathbf{p}$ are evaluated.

Notice that the last entry of the vector $\mathbf{p}$, corresponding to the RHS of (24), vanishes for the field φ:

$$\frac{1}{2} \int_{\partial\Sigma} (\mathbf{r} \cdot \mathbf{r}) \boldsymbol{\omega} \cdot \mathbf{n}_\partial \, \mathrm{d}s = -\frac{1}{2} \int_{\partial\Sigma} (\mathbf{r} \cdot \mathbf{r}) \mathbf{r}^{\perp} \cdot \mathbf{n}_\partial \, \mathrm{d}s = \mathbf{o} \, . \tag{46}$$

Actually, assuming that each boundary of the multiply-connected domain is a curve parameterized with respect to its length, the tangent vector is given by

$$\mathbf{t}_\partial = \frac{\partial \mathbf{r}(s)}{\partial s} \, ,$$

so that, being $\mathbf{n}_\partial = -\mathbf{t}_\partial^{\perp}$, one has

$$(\mathbf{r} \cdot \mathbf{r}) \mathbf{r}^{\perp} \cdot \mathbf{n}_\partial = -(\mathbf{r} \cdot \mathbf{r}) \mathbf{r} \cdot \mathbf{t}_\partial = -(\mathbf{r} \cdot \mathbf{r}) \mathbf{r} \cdot \frac{\partial \mathbf{r}}{\partial s} = -\frac{1}{2} (\mathbf{r} \cdot \mathbf{r}) \frac{\partial (\mathbf{r} \cdot \mathbf{r})}{\partial s} = -\frac{1}{4} \frac{\partial (\mathbf{r} \cdot \mathbf{r})^2}{\partial s} \, .$$

This means that the integrand function in (46) is an exact differential and the line integral, being evaluated along closed curves $\partial\Sigma_b$, vanishes.

4.2. Evaluation of the vector $\mathbf{p}$ for the harmonic vector field $\boldsymbol{\psi}$

Although we are dealing with a vector field, the analysis presented for the general case (5) is still valid for the evaluation of the function $\boldsymbol{\psi}$. Actually, it is convenient to analyze separately the two components of the vector $\boldsymbol{\psi}$, namely ψ_x and ψ_y, and consider two distinct Neumann problems:

$$\begin{cases} \psi_x \nabla^2 = 0 \, , & \forall \mathbf{r} \in \Sigma \, , \\ \psi_x \nabla \cdot \mathbf{n}_\partial = -\mathbf{a}_x \cdot \mathbf{n}_\partial \, , & \forall \mathbf{r} \in \partial\Sigma \, , \end{cases} \tag{47a}$$

$$\begin{cases} \psi_y \nabla^2 = 0 \, , & \forall \mathbf{r} \in \Sigma \, , \\ \psi_y \nabla \cdot \mathbf{n}_\partial = -\mathbf{a}_y \cdot \mathbf{n}_\partial \, , & \forall \mathbf{r} \in \partial\Sigma \, , \end{cases} \tag{47b}$$

in which $\mathbf{a}_x$ and $\mathbf{a}_y$ are two vectors whose components coincide with the rows of $\mathbf{A}$:

$$[\mathbf{A}] = \begin{bmatrix} \mathbf{a}_x^T \\ \mathbf{a}_y^T \end{bmatrix} . \tag{48}$$

This ensures that

$$\mathbf{a}_x \cdot \mathbf{n}_\partial = (\mathbf{A}\mathbf{n}_\partial)_x \, , \quad \mathbf{a}_y \cdot \mathbf{n}_\partial = (\mathbf{A}\mathbf{n}_\partial)_y \, , \tag{49}$$

so that both (47a) and (47b) stem from (5) by setting $\boldsymbol{\omega} = -\mathbf{a}_x$ and $\boldsymbol{\omega} = -\mathbf{a}_y$, respectively.

In order to evaluate the column vector $\mathbf{p}$ of the linear system (22), to be associated both with (47a) and (47b), let us first consider the expression of $\mathbf{A}\mathbf{n}_\partial$ relevant to the i-th edge of the boundary. Recalling (3), one has

$$\mathbf{A}_i(\mu)\mathbf{n}_{\partial i} = \frac{1+\bar{\nu}}{4} \left[\mathbf{r}_i(\mu) \cdot \mathbf{n}_{\partial i} \right] \mathbf{r}_i(\mu) + \frac{1-3\bar{\nu}}{8} \left[\mathbf{r}_i(\mu) \cdot \mathbf{r}_i(\mu) \right] \mathbf{n}_{\partial i} \, ,$$

and, by means of (27), (29) and (40), the following expression is obtained:

$$\mathbf{A}_i(\mu)\mathbf{n}_{\partial i} = \frac{1}{2 l_i} \left[\frac{1+\bar{\nu}}{4} \lambda_i (\boldsymbol{\beta}_i + \boldsymbol{\alpha}_i \mu) + - \frac{1-3\bar{\nu}}{16} (\boldsymbol{\beta}_i \cdot \boldsymbol{\beta}_i + 2 \boldsymbol{\alpha}_i \cdot \boldsymbol{\beta}_i \mu + \boldsymbol{\alpha}_i \cdot \boldsymbol{\alpha}_i \mu^2) \boldsymbol{\alpha}_i^{\perp} \right] , \tag{50}$$

where $\boldsymbol{\alpha}_i$ and $\boldsymbol{\beta}_i$ are defined by (28).

Component ψ_x Since the function $\psi_x(\mathbf{r})$ is defined through the differential problem (47a), we set $\boldsymbol{\omega} = -\mathbf{a}_x$ so that, by using $(49)_1$, the RHS of (22) becomes

$$-\sum_{i=1}^{N} l_i \int_{-1}^{1} \ln \left\| \mathbf{r}_i(\mu) - \mathbf{r}_{h_l}^* \right\|^2 \boldsymbol{\omega}_i(\mu) \cdot \mathbf{n}_{\partial i} \, \mathrm{d}\mu = \sum_{i=1}^{N} l_i \int_{-1}^{1} \ln \left\| \mathbf{r}_i(\mu) - \mathbf{r}_{h_l}^* \right\|^2 [\mathbf{A}_i(\mu)\mathbf{n}_{\partial i}]_x \, \mathrm{d}\mu \, .$$

Recalling (35) and considering the first component of the vector evaluated in (50) one has

$$\sum_{i=1}^{N} l_i \int_{-1}^{1} \ln \left\| \mathbf{r}_i(\mu) - \mathbf{r}_{h_l}^* \right\|^2 [\mathbf{A}_i(\mu)\mathbf{n}_{\partial i}]_x \, \mathrm{d}\mu = \frac{1}{2} \sum_{i=1}^{N} \int_{-1}^{1} \ln (b_i \mu^2 + c_i^* \mu + d_i^*)(F_i + G_i \mu + H_i \mu^2) \, \mathrm{d}\mu \, ,$$

being

$$\begin{aligned} F_i &= \frac{1+\bar{\nu}}{4} \lambda_i \beta_{xi} + \frac{1-3\bar{\nu}}{16} (\boldsymbol{\beta}_i \cdot \boldsymbol{\beta}_i) \alpha_{yi} \, , \\ G_i &= \frac{1+\bar{\nu}}{4} \lambda_i \alpha_{xi} + \frac{1-3\bar{\nu}}{8} (\boldsymbol{\alpha}_i \cdot \boldsymbol{\beta}_i) \alpha_{yi} \, , \\ H_i &= \frac{1-3\bar{\nu}}{16} (\boldsymbol{\alpha}_i \cdot \boldsymbol{\alpha}_i) \alpha_{yi} \, . \end{aligned} \tag{51}$$

where definitions (28) of the vectors $\boldsymbol{\alpha}_i$ and $\boldsymbol{\beta}_i$ have been used, along with the corresponding components on x-axis and y-axis. Finally, formula (9.5) of the supplementary material [62] is applied to evaluate the integral:

$$\frac{1}{2} \sum_{i=1}^{N} \int_{-1}^{1} \ln (b_i \mu^2 + c_i^* \mu + d_i^*)(F_i + G_i \mu + H_i \mu^2) \, \mathrm{d}\mu = \frac{1}{2} \sum_{i=1}^{N} \left[F_i L_0(b_i, c_i^*, d_i^*) + G_i L_1(b_i, c_i^*, d_i^*) + H_i L_2(b_i, c_i^*, d_i^*) \right] . \tag{52}$$

The last element of the vector $\mathbf{p}$ is expressed by the RHS of (25), which is explicitly written by means of (27) and considering the first component of the vector (50):

$$\begin{aligned}
&\frac{1}{2}\sum_{i=1}^{N} l_i \int_{-1}^{1} [\mathbf{r}_i(\mu)\cdot\mathbf{r}_i(\mu)]\boldsymbol{\omega}_i(\mu)\cdot\mathbf{n}_{\partial i}\,\mathrm{d}\mu \\
&= -\frac{1}{2}\sum_{i=1}^{N} l_i \int_{-1}^{1} [\mathbf{r}_i(\mu)\cdot\mathbf{r}_i(\mu)][\mathbf{A}_i(\mu)\mathbf{n}_{\partial i}]_x\,\mathrm{d}\mu \\
&= -\frac{1}{16}\sum_{i=1}^{N} (U_i P_0 + V_i P_2 + W_i P_4)\,,
\end{aligned} \tag{53}$$

where we have set

$$\begin{aligned}
&U_i = (\boldsymbol{\beta}_i\cdot\boldsymbol{\beta}_i)F_i\,, \qquad V_i = (\boldsymbol{\alpha}_i\cdot\boldsymbol{\alpha}_i)F_i + 2(\boldsymbol{\alpha}_i\cdot\boldsymbol{\beta}_i)G_i + (\boldsymbol{\beta}_i\cdot\boldsymbol{\beta}_i)H_i\,, \\
&W_i = (\boldsymbol{\alpha}_i\cdot\boldsymbol{\alpha}_i)H_i\,,
\end{aligned} \tag{54}$$

being the parameters F_i, G_i and H_i evaluated through (51). Please notice that the addends involving μ and μ^3 and the relevant coefficients have been omitted since, by means of formula (9.2) of the supplementary material [62], P_n vanishes when n is odd.

Component ψ_y

The field $\psi_y(\mathbf{r})$ is the solution to the Neumann problem (47b), so that we set $\boldsymbol{\omega} = \mathbf{a}_y$. The RHS of (22) by means of $(49)_2$ becomes

$$\begin{aligned}
&-\sum_{i=1}^{N} l_i \int_{-1}^{1} \ln\left\|\mathbf{r}_i(\mu)-\mathbf{r}^*_{h_l}\right\|^2 \boldsymbol{\omega}_i(\mu)\cdot\mathbf{n}_{\partial i}\,\mathrm{d}\mu \\
&= \sum_{i=1}^{N} l_i \int_{-1}^{1} \ln\left\|\mathbf{r}_i(\mu)-\mathbf{r}^*_{h_l}\right\|^2 [\mathbf{A}_i(\mu)\mathbf{n}_{\partial i}]_y\,\mathrm{d}\mu\,.
\end{aligned}$$

The same strategy used for ψ_x is applied, obtaining the following expression

$$\begin{aligned}
&\sum_{i=1}^{N} l_i \int_{-1}^{1} \ln\left\|\mathbf{r}_i(\mu)-\mathbf{r}^*_{h_l}\right\|^2 [\mathbf{A}_i(\mu)\mathbf{n}_{\partial i}]_y\,\mathrm{d}\mu \\
&= \frac{1}{2}\sum_{i=1}^{N}\left[F_i L_0(b_i,c_i^*,d_i^*) + G_i L_1(b_i,c_i^*,d_i^*) + H_i L_2(b_i,c_i^*,d_i^*)\right],
\end{aligned}$$

where the parameters F_i, G_i and H_i this time are evaluated as

$$\begin{aligned}
F_i &= \frac{1+\bar{\nu}}{4}\lambda_i\beta_{y_i} - \frac{1-3\bar{\nu}}{16}(\boldsymbol{\beta}_i\cdot\boldsymbol{\beta}_i)\alpha_{x_i}\,, \\
G_i &= \frac{1+\bar{\nu}}{4}\lambda_i\alpha_{y_i} - \frac{1-3\bar{\nu}}{8}(\boldsymbol{\alpha}_i\cdot\boldsymbol{\beta}_i)\alpha_{x_i}\,, \\
H_i &= -\frac{1-3\bar{\nu}}{16}(\boldsymbol{\alpha}_i\cdot\boldsymbol{\alpha}_i)\alpha_{x_i}\,,
\end{aligned} \tag{55}$$

since the second component of the vector (50) must be used.

The last component of the vector $\mathbf{p}$ derives from the RHS of (25) and is estimated through a formula analogous to (53):

$$\begin{aligned}
&\frac{1}{2}\sum_{i=1}^{N} l_i \int_{-1}^{1} [\mathbf{r}_i(\mu)\cdot\mathbf{r}_i(\mu)]\boldsymbol{\omega}_i(\mu)\cdot\mathbf{n}_{\partial i}\,\mathrm{d}\mu \\
&= -\frac{1}{2}\sum_{i=1}^{N} l_i \int_{-1}^{1} [\mathbf{r}_i(\mu)\cdot\mathbf{r}_i(\mu)][\mathbf{A}_i(\mu)\mathbf{n}_{\partial i}]_y\,\mathrm{d}\mu \\
&= -\frac{1}{16}\sum_{i=1}^{N} (U_i P_0 + V_i P_2 + W_i P_4)\,,
\end{aligned} \tag{56}$$

where U_i, V_i and W_i are evaluated by means of (54) but using the values (55) of the parameters F_i, G_i, H_i.

5. Some general issues concerning the numerical analysis

Given a polygonal domain having n edges, one fixes the number m_k of elements for the k-th edge along with the number of polynomial coefficients q_i for the i-th boundary element. In line of principle, an arbitrary partition of the boundary could be used, as well as polynomial functions having different degrees for each element. However, such a choice can be reasonable only on a problem-at-hand basis.

The simplest strategy is that of considering the same number q of coefficients for each element's polynomial:

$$q_i = q\,, \quad i = 1,\ldots,N\,. \tag{57}$$

where N is the total number of boundary elements.

However a large number of numerical experiments, only partially documented in Section 6 due to space limitations, has shown that it is convenient to adopt a partition as much uniform as possible. To this end we introduce the discretization parameter m representing the number of elements pertaining to the edge having the minimum length $l_{\min}$. Hence, for the k-th edge the number of elements is evaluated as

$$m_k = \left\lceil m\frac{l_k}{l_{\min}}\right\rceil, \quad k = 1,\ldots,n\,, \tag{58}$$

in which l_k is the length of the k-th edge of the boundary and n is the total number of edges.

Some preliminary tests have shown that the size of the domain can influence the numerical stability of the recursive formulas reported in section 9 of the supplementary material [62]. Such instability is due to rounding in calculating the coefficients a, b and c involved in formulas (9.3), (9.4) and (9.5) in [62], despite their analytical validity.

In order to avoid such a drawback, the vectors $\mathbf{r}_k$ defining the domain vertices are scaled by a factor f_s and then the minimum length edge is divided into m elements having a fixed length l_{ref}:

$$\frac{f_s l_{\min}}{m} = l_{\text{ref}}\,. \tag{59}$$

It has emerged from our tests that round-off errors do not affect the usability of the recursive formulas (9.3), (9.4) and (9.5) in [62] if the length of each boundary element is between 0.1 and 10. For this reason we fix $l_{\text{ref}} = 1$, implying the length of each boundary element to be between 0.5 and 1. The procedure implementing the scaling and the discretization of the boundary is summarized in the Algorithm 1. included in the supplementary material [62].

Once the domain geometry has been scaled by f_s, the procedure described in Section 2 yields a solution to the Neumann problem (5) for the real domain provided that the coefficients $a_p^{(i)}$, defining the interpolating functions $\Gamma_i(\mu)$, are divided by a suitable factor f_Γ depending on the dimensions of the field Γ.

Specifically, with reference to the fields φ and $\boldsymbol{\psi}$, defined by the Neumann problems (1) and (2), we introduce the following function scale factors:

$$f_\varphi = f_s^2\,, \qquad f_{\psi_x} = f_{\psi_y} = f_s^3\,,$$

since the unknown functions have the dimensions of a length to the power of 2, regarding φ, and to the power of 3, as far as the components ψ_x and ψ_y of the vector field $\boldsymbol{\psi}$ are concerned.

It is worth being emphasized that the assumptions on the polynomial degrees and the boundary discretization, defined through (57) and (58) respectively, make q and m the parameters governing the accuracy of the numerical solution to the problem (5). In particular, we will show in Section 5.1 how these parameters influence the reliability of the numerical results and we will also discuss a criterion to set them.

At the same time the numerical tests reported in Section 6 will provide some indications on the value of m and q to be adopted with the specific reference to the harmonic fields φ and $\boldsymbol{\psi}$.

5.1. *Optimal choice of the parameters for the numerical solution*

On account of assumptions (57) and (58), the parameters influencing the numerical results in solving the Neumann problem (5) are the number of elements m of the minimum length edge and the number of coefficients q of the interpolating polynomial for each element.

In principle, an improvement in the accuracy of the solution can be achieved by increasing either q or m, since in both cases the total number

M of parameters describing the numerical solution would increase. In this respect we recall that definition (17) of M specifies in

$$M = q \cdot N ,$$

being N the number of boundary elements resulting from the discretization associated with m.

However, some preliminary tests have shown an instability in the numerical procedure when, for a fixed discretization of the boundary, the degree of the interpolating polynomial increases. Moreover, the value of q above which the results become not reliable is strictly related to the input data, such as the shape of the domain. Hence it is not possible to provide a general indication about the best value to assign to the degree of the interpolating polynomials.

Nevertheless, we can exploit a continuity condition of the interpolating polynomials in order to obtain an index of accuracy of the solution, to be associated with the parameters q and m.

We have emphasized in Section 2.3 that the Chebyshev nodes are used in evaluating the coefficients defining the polynomials $\Gamma_i(\mu)$, so that the elements' extremities are excluded from the set of collocation points. However we recall that the function Γ is required to be at least twice continuously differentiable on Σ and once on $\partial\Sigma$, so that it is possible to exploit the C^0 continuity at the extremities of the elements in order to estimate the accuracy of the numerical solution.

Let $\Delta\Gamma_i$ be the difference between the interpolating functions at the i-th point of the discretized boundary, i.e. a node common to two consecutive elements:

$$\Delta\Gamma_i = |\Gamma_i(-1) - \Gamma_{i-1}(1)| , \quad i = 1, \dots, N , \tag{60}$$

being $\Gamma_i(\mu)$ the interpolating polynomial on the i-th boundary element. The average continuity error along the boundary is obtained by dividing the sum of the local errors $\Delta\Gamma_i$ by the total number of points N. Moreover, in order to obtain a normalized mean error, we also divide the resulting value by a proper parameter α_Γ, depending on the specific Neumann problem:

$$e = \frac{1}{\alpha_\Gamma N} \sum_{i=1}^{N} \Delta\Gamma_i . \tag{61}$$

Since φ and the components ψ_x and ψ_y of $\boldsymbol{\psi}$ have the dimension of a length to the power of 2 and 3, respectively, we set

$$\alpha_\varphi = d_{\text{sec}}^2 , \qquad \alpha_{\psi_x} = \alpha_{\psi_y} = d_{\text{sec}}^3 , \tag{62}$$

where d_{sec} is the characteristic dimension of the domain Σ, assumed to be represented by the square root of the area A.

5.2. Convergence algorithms

It has been already emphasized that, for a fixed boundary discretization defined through m, the numerical solution for the problem (5), reduced to the linear system (26), cannot be found for any number q of the polynomial parameters. However, for each boundary partition, it is possible to define a limit value $\bar{q}$ above which the numerical solution of (26) cannot be considered reliable or cannot be found at all because of the round-off approximation.

Thus we are going to show that it is possible to exploit the continuity error e defined by (61) to find the limit value of q associated with a given boundary discretization.

To this end let us assign a value to m, identifying a boundary discretization for the domain, and estimate the accuracy of the numerical solution associated with increasing values of q. We expect that the continuity error e decreases as the accuracy of the solution improves. Thus, supposing to gradually increase the degree of the interpolating polynomial, e decreases until it reaches a minimum at a certain value of q. The subsequent growing of e is interpreted as an indication that the limit of stability of the algorithm has been reached for the assigned value of m.

We identify $\bar{q}(m)$ as the value corresponding to a minimum in e, i.e.

$$\begin{cases} e(m, q) < e(m, q-1) , & \forall q \in \{2, \dots, \bar{q}\} , \\ e(m, \bar{q}) \le e(m, \bar{q}+1) , \end{cases} \tag{63}$$

and $\bar{e}(m)$ as the relevant limit value of the mean continuity error:

$$\bar{e}(m) = e(m, \bar{q}) . \tag{64}$$

The numerical solutions corresponding to $q > \bar{q}$ are judged to be not conveniently accurate, so that a further improvement in the accuracy can be obtained only by increasing the parameter m, i.e. by applying a finer discretization of the boundary $\partial\Sigma$.

By considering $\bar{q}$ as a function of m, it is possible to define a border in the m-q plane which separates the stability region from the instability one. Only the points (m, q) within the stability region can be properly used for an accurate numerical estimation of the warping functions φ, ψ_x and ψ_y.

The continuity mean error is exploited not only for the determination of the stability region, but also for implementing a convergence criterion aimed at finding a sufficiently accurate numerical solution. Indeed, once an acceptable tolerance ε is fixed, several combinations of m and q can be explored until it is found a value for e which is lower than ε.

In the following sections we describe three procedures that can be easily implemented for the detection of the desired solution. Actually, the numerical tests reported in Section 6 allow one to derive some guidance in setting the parameters m and q both for compact domains and for thin-walled domains, avoiding to perform this preliminary analysis.

5.2.1. Bottom-up (BU) algorithm

The simplest approach to find the limit value $\bar{q}$ and the corresponding continuity error $\bar{e}$ is to assign a value to m and progressively increment q, starting from $q = 2$, until the criterion (63) is complied and the corresponding error is obtained. The procedure is summarized in the Algorithm 2, included in the supplementary material [62].

The optimal value $\bar{q}$ is determined by examining the solutions and related errors associated with values of q in the range $[2, \bar{q}+1]$ till when a change of trend is detected for the values of e. In particular, Algorithm 2 is recursively invoked in the procedure related to the detection of the pair (m, q) providing a sufficiently accurate solution of the Neumann problem, see, e.g. Algorithm 3 in the supplementary material [62].

Specifically, we start by setting $m = 1$ and estimating the limit value of q, by means of the Algorithm 2, as well as the corresponding continuity error $\bar{e}$. If $\bar{e}$ is greater than the fixed tolerance, m is incremented by 1 and Algorithm 2 is applied again. This procedure is recursively repeated until a pair (m, q) is found such that the corresponding error satisfies $e \le \varepsilon$. It has to be noted that since at each step the continuity error is evaluated within the stability region, if a value for e lower than the tolerance is found, the procedure can be stopped without the detection of $\bar{q}$.

5.2.2. Top-down (TD) algorithm

The approach based on the BU algorithm requires the evaluation of all the possible solutions within the stability region, until one corresponding to the desired accuracy is found. This procedure, although accurate, can result very slow for domains characterized by high values of $\bar{q}$.

A more efficient algorithm can be implemented if we take into account that $\bar{q}$ decreases with respect to m:

$$\bar{q}(m) \le \bar{q}(m-1) . \tag{65}$$

This particular feature of the stability border, emerging from the numerical tests on several domains, is justified by the fact that the reliability of the numerical solution turns out to be undetermined when the total number of the parameters arbitrarily increases. Thus, as the number of the boundary elements increases, the maximum degree of the interpolating polynomial that can be efficiently associated with each element reduces.

Supposing that the discretization corresponding to m has been fixed, the limit value $\bar{q}(m-1)$ provides an upper bound for the set of values containing $\bar{q}(m)$. From this point of view, in order to find the limit value for the current discretization, it is possible to progressively reduce q starting from $q_{\text{sup}}(m) = \bar{q}(m-1)$ until a minimum in e is found:

$$\begin{cases} e(m, q-1) < e(m, q)\,, \quad \forall q \in \{\bar{q}, \ldots, q_{\text{sup}}\}\,, \\ e(m, \bar{q}) \leq e(m, \bar{q}-1)\,. \end{cases} \tag{66}$$

By exploiting criterion (66), the procedure detecting $\bar{q}$ can by implemented as described in the Algorithm 4 in the supplementary material [62].

The TD algorithm can be used in place of the BU algorithm in the recursive procedure finalized to the detection of the pairs (m, q) such that the corresponding error satisfies the convergence criterion $e \leq \varepsilon$.

As shown in the Algorithm 5, see e.g. the supplementary material [62], at the first step the BU algorithm is required since there is no information about the extension of the stability region. Once the value of $\bar{q}$ corresponding to $m = 1$ is obtained, this can be used as the upper bound of the unknown $\bar{q}$ in the subsequent analysis to be carried out by the TD algorithm, and so on until the convergence criterion is satisfied.

Please notice that Algorithm 5 only considers the pairs (m, q) near the border of the stability region. As a consequence, it may happen that there exists a solution satisfying the convergence criterion which is located in the interior of the stability region and that is characterized by a lower number of parameters than the ones detected by the TD algorithm.

Avoiding the analysis of all points of the stability region, the TD algorithm results to be really time-saving, since the analysis of each pair (m, q) requires the assembling and the solution of the algebraic problem (26), thus making the detection of a suitable solution (m, q) the most expensive part of the overall process.

5.2.3. Pseudo-tangent procedure

The procedures described by Algorithms 3 and 5 both consider a discretization of the boundary that becomes denser and denser by increasing by 1 the parameter m at each step, until a value allowing to find a continuity error compatible with the fixed tolerance is reached. Such a method implies the analysis of the whole stability region, with regard to the BU approach, or at least its limit line, as regards the TD approach, until a satisfactory solution is found.

However, with the aim of detecting a pair (m, q) suitable to provide a sufficiently accurate numerical solution, we do not need to analyze all the possible discretizations. Actually our aim is to identify a value for m which provides an appropriate discretization avoiding, when it is possible, the analyses associated with the intermediate values.

To this end we consider the continuity error $\bar{e}$ at the limit of stability as a function of the discretization parameter m and let ε be the fixed tolerance. Our purpose is to find the value m^* of m such that

$$\bar{e}(m^*) \leq \varepsilon\,. \tag{67}$$

Let us suppose that two consecutive points of the stability border have been detected, so that the errors $\bar{e}_{m-1} = \bar{e}(m-1)$ and $\bar{e}_m = \bar{e}(m)$ have been evaluated. We replace the unknown function $\bar{e}$ with its linear approximation at the point $(m, \bar{e}_m)$, so that condition (67), considered with the equal sign, becomes

$$\bar{e}(m^*) \approx \bar{e}_m - \left(\frac{\bar{e}_{m-1} - \bar{e}_m}{1}\right)\Delta m = \varepsilon\,; \tag{68}$$

this allows us to obtain the increment Δm for the parameter m as

$$\Delta m = \left\lceil \frac{\bar{e}_m - \varepsilon}{\bar{e}_{m-1} - \bar{e}_m} \right\rceil, \tag{69}$$

where the ceiling function, represented through the symbol $\lceil\cdot\rceil$, has been used since m is a discrete variable.

This approach can be seen as a sort of tangent method for the resolution of Eq. (67). However, since m is not a continuous variable, the derivative of the function $\bar{e}(m)$ is not defined, so that the linear approximation appearing in (68) can be interpreted as the equation of the pseudo-tangent to the stability limit line at the point $(m, \bar{e}_m)$.

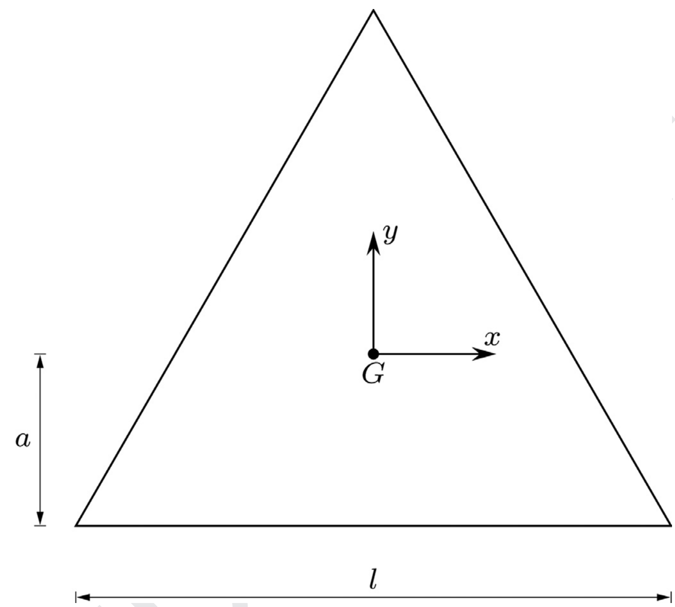

Fig. 2. Triangular domain.

Clearly, formula (68), and hence formula (69), has been obtained considering two consecutive values of the limit error $\bar{e}(m)$, so it can be applied only if at the previous step the increment of m is 1. Moreover, although the overall trend of the line $\bar{e}(m)$ is a decreasing one, the continuity error can locally increase, producing $\bar{e}_{m-1} \leq \bar{e}_m$. In such a case formula (69) cannot be applied and we simply set $\Delta m = 1$.

The implementation of the pseudo-tangent procedure is described by Algorithm 6 in the supplementary material [62]. If compared to Algorithm 5 it is evident that the only difference is the evaluation of the increment Δm, an adjustment that, however, makes the procedure much more effective.

6. Numerical tests

To prove the effectiveness of the numerical procedures described in the previous sections we show the numerical results obtained with reference to several domains, with special emphasis on the thin-walled ones since they undoubtedly are the most challenging ones.

6.1. Triangular domain

The first analysis we consider as benchmark concerns the evaluation of the φ field for the equilateral triangle shown in Fig. 2. In such case, the warping function can be expressed in closed form (see [1]) as

$$\varphi(x, y) = \frac{1}{6a}\left(3xy^2 - x^3\right) = \frac{\sqrt{3}}{3l}\left(3xy^2 - x^3\right). \tag{70}$$

In order to make a comparison with the numerical solution of the problem (1), we derive the restriction of φ at the boundary. In particular, with reference to the horizontal edge, by replacing $y = -a$ in (70), we obtain

$$\varphi_1(x) = \frac{1}{6a}\left(3a^2 x - x^3\right),$$

an expression that becomes, in terms of normalized abscissa μ,

$$\varphi_1(\mu) = \frac{\sqrt{3}l^2}{24}\left(\mu - \mu^3\right), \quad \mu \in [-1, 1]. \tag{71}$$

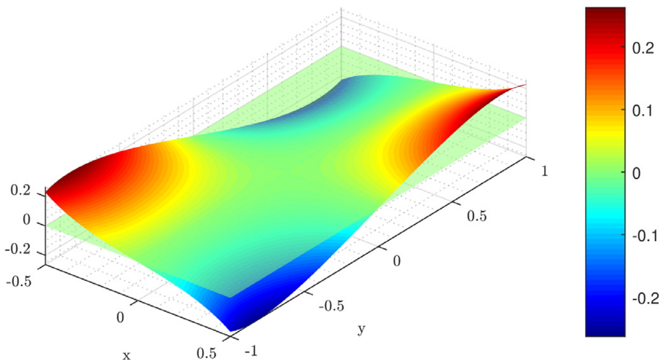

Fig. 3. Torsional warping function φ for a rectangular domain ($B = 1$, $H = 2$).

Please notice that, because of the symmetries of the domain, in terms of local abscissa μ the expressions of $\varphi_2(\mu)$ and $\varphi_3(\mu)$ are the same as $\varphi_1(\mu)$.

As far as concerns the numerical solution, since it is known from (71) that $\varphi_1(\mu)$ is a third degree polynomial, we consider $l = 1$ and we simply set $m_i = m = 1$ and $q = 4$ for the procedure described in Section 2.2; hence, the following values for the polynomial coefficients $a_p^{(i)}$ are obtained:

$$a_1^{(i)} = 0.000000\,, \quad a_2^{(i)} = 0.072169\,, \quad a_3^{(i)} = 0.000000\,, \quad a_4^{(i)} = -0.072169\,,$$

which exactly coincide with the analytical solution (71).

It is worth noting that the example here described represents the counterpart of the standard patch test in the finite element method. Actually, since the analytical solution consists of polynomial functions of degree 3, it can be completely reproduced by the numerical solution by setting $q = 4$, what implies the solution to be searched in the set of the third degree polynomials.

6.2. Rectangular domain

Let us evaluate the torsional warping function φ for a rectangular domain having base B and height H.

Unlike the case of the equilateral triangle, for the rectangular domain the analytical solution of the field φ is not available in closed form. However it can be estimated by means of the following series expansion [1]:

$$\begin{aligned}\varphi(x, y) &= -xy + H^2\left(\frac{2}{\pi}\right)^3 \sum_{n=0}^{\infty} f_n(x, y)\\ &= -xy + H^2\left(\frac{2}{\pi}\right)^3 \sum_{n=0}^{\infty} \frac{(-1)^n}{(2n+1)^3} \frac{\sinh\frac{(2n+1)\pi x}{H}}{\cosh\frac{(2n+1)\pi B}{2H}} \sin\frac{(2n+1)\pi y}{H}\,,\end{aligned} \tag{72}$$

whose graphical representation is shown in Fig. 3 referring to $B = 1$ and $H = 2$. Please notice that in evaluating $\varphi(x, y)$ the series appearing in (72) has been truncated at the N-th term such that

$$\left|\frac{F_N(x,y) - F_{N-1}(x,y)}{F_N(x,y)}\right| = \left|\frac{f_n(x,y)}{F_N(x,y)}\right| \le 10^{-16}\,,$$

where

$$F_N(x, y) = \sum_{n=0}^{N} f_n(x, y)\,.$$

At the same time, specializing expression (14) to the field φ one has

$$\begin{aligned} c(\mathbf{r}^*)\varphi(\mathbf{r}^*) - \frac{1}{2\pi}\sum_{i=1}^{N}\frac{l_i}{2}\int_{-1}^{1}\varphi_i(\mu)\frac{[\mathbf{r}_i(\mu)-\mathbf{r}^*]\cdot\mathbf{n}_{\partial i}}{\|\mathbf{r}_i(\mu)-\mathbf{r}^*\|^2}\,\mathrm{d}\mu \\ = \frac{1}{2\pi}\sum_{i=1}^{N}\frac{l_i}{2}\int_{-1}^{1}\ln\|\mathbf{r}_i(\mu)-\mathbf{r}^*\|\mathbf{r}_i^{\perp}(\mu)\cdot\mathbf{n}_{\partial i}\,\mathrm{d}\mu\,, \end{aligned}$$

yielding, on account of (15) specialized to $\varphi_i(\mu)$, the value of the harmonic function at the arbitrary point $\mathbf{r}^*$:

$$\begin{aligned} c(\mathbf{r}^*)\varphi(\mathbf{r}^*) = \frac{1}{4\pi}\sum_{i=1}^{N} l_i\Bigg[\sum_{p=1}^{q_i} a_p^{(i)}\int_{-1}^{1}\mu^{p-1}\frac{[\mathbf{r}_i(\mu)-\mathbf{r}^*]\cdot\mathbf{n}_{\partial i}}{\|\mathbf{r}_i(\mu)-\mathbf{r}^*\|^2}\,\mathrm{d}\mu \\ + \int_{-1}^{1}\ln\|\mathbf{r}_i(\mu)-\mathbf{r}^*\|\mathbf{r}_i^{\perp}(\mu)\cdot\mathbf{n}_{\partial i}\,\mathrm{d}\mu\Bigg]\,. \end{aligned} \tag{73}$$

The two integrals appearing in (73) can be evaluated retracing the procedures described in Sections 3 and 4.1, respectively. Moreover, it is worth noting that, in order to obtain the value of the field φ at $\mathbf{r}^*$, the weak form (73) is not required if $\mathbf{r}^*$ belongs to the boundary $\partial\Sigma$ of the domain since the polynomial approximation (15) can be directly applied for each boundary element. Consequently, recalling from (9) that $c(\mathbf{r}^*) = 1$ for any interior point, the values of the harmonic function φ are obtained as

$$\begin{aligned} \varphi(\mathbf{r}^*) = \frac{1}{4\pi}\sum_{i=1}^{N}\Bigg[e_i^*\sum_{p=1}^{q_i} a_p^{(i)} M_{p-1}(b_i, c_i^*, d_i^*) + \\ -\frac{f_i}{4}L_0(b_i, c_i^*, d_i^*) - \frac{g_i}{4}L_1(b_i, c_i^*, d_i^*)\Bigg]\,, \quad \forall \mathbf{r}^* \in \mathring{\Sigma}\,, \end{aligned} \tag{74}$$

$$\varphi(\mathbf{r}^*) = \varphi_i(\mu_i^*) = \sum_{p=1}^{q_i} a_p^{(i)} \mu_i^{*\,p-1}\,, \quad \forall \mathbf{r}^* \in \partial\Sigma_i\,,\ i = 1, \ldots, N\,. \tag{75}$$

The parameters b_i, c_i^*, d_i^*, e_i^*, f_i and g_i in (74) are evaluated by means of 31–(34) and (43), while M_n and L_n are provided by the recursive formulas (9.4) and (9.5) in [62]. Furthermore, in Eq. (75), the abscissa μ_i^* relevant to the point $\mathbf{r}^*$ belonging to the i-th element is expressed as

$$\mu_i^* = \frac{(2\mathbf{r}^* - \boldsymbol{\beta}_i)\cdot\boldsymbol{\alpha}_i}{l_i^2}\,, \tag{76}$$

where $\boldsymbol{\alpha}_i$ and $\boldsymbol{\beta}_i$ are given by (28) and l_i is the length of the i-th boundary element.

In order to evaluate the coefficients $a_p^{(i)}$, Algorithm 6 has been applied considering a tolerance $\varepsilon = 10^{-8}$ for the continuity error e. The convergence has been attained at $m = 33$, corresponding to a total number of boundary elements $N = 198$, and $q = 7$.

The values provided by 74–(75) can be compared with the ones evaluated by using (72), to be considered as reference $\varphi_{\mathrm{ref}}(\mathbf{r}^*)$. The comparison is shown in Fig. 4 in terms of relative error respect to $\bar{\varphi}$, representing the mean of the absolute value of $\varphi_{\mathrm{ref}}(\mathbf{r}^*)$ over the domain

$$err(\mathbf{r}^*) = \frac{|\varphi(\mathbf{r}^*) - \varphi_{\mathrm{ref}}(\mathbf{r}^*)|}{\bar{\varphi}}\,, \tag{77}$$

resulting at most of order of 10^{-6}.

6.3. Doubly-connected domain

The convergence criterion for the numerical solution of the Neumann problem requires the continuity error e to be lower than a fixed tolerance ε. However the extensive numerical tests that we have carried out have shown that a very large number of parameters could be required in order to reach the desired tolerance, depending on the shape of the domain.

For this reason, a limit value M_{lim} of the total number of parameters is introduced such that the analysis stops before that the convergence criterion on the continuity error is satisfied. In fact, once m has been fixed and the number of elements N has been derived by Algorithm 1, the limit value of q compatible with M_{lim} is given by

$$q_{\mathrm{lim}} = \lfloor M_{\mathrm{lim}}/N \rfloor\,. \tag{78}$$

If the point (m, q_{lim}) is outside the stability region, the standard procedure can be applied, either by means of Algorithm 2 or Algorithm 4. Otherwise, q_{lim} provides the maximum value of q which actually can be considered and it can happen that $e(m, q_{\mathrm{lim}}) > \varepsilon$. This means that the

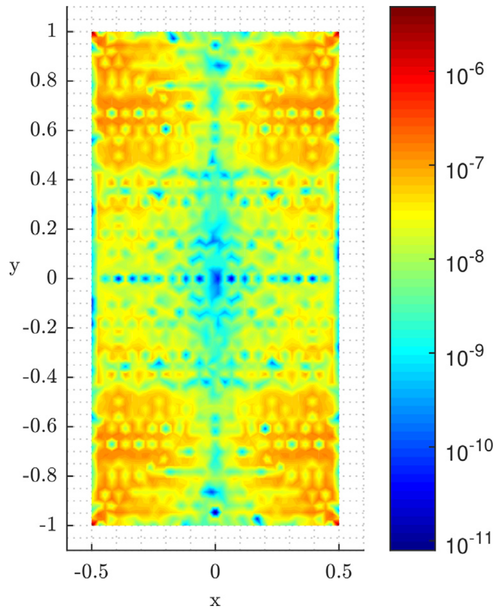

Fig. 4. Relative error of φ for a rectangular domain ($B = 1$, $H = 2$).

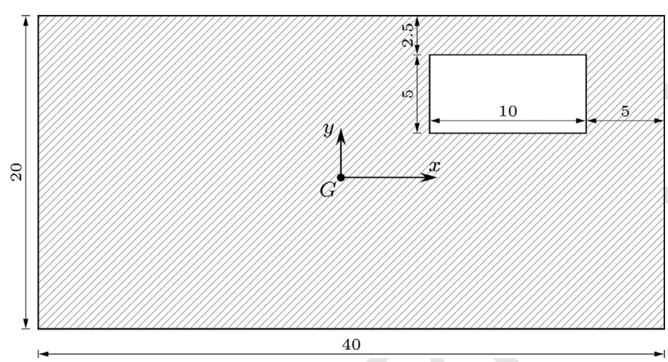

Fig. 5. Doubly-connected domain.

continuity error e decreases too slowly and the convergence criterion $e \leq \varepsilon$ cannot be satisfied in accordance with M_{lim}.

Since the increasing of m, and consequently N, implies a progressive reduction of q_{lim} on account of (78), further combinations of m and q_{lim} can be explored until the minimum value $q_{\text{lim}} = 2$ is reached. Accordingly, the solution to be adopted is the one corresponding to the minimum value of e.

An example of analysis governed by the number of parameters rather than the tolerance is given by the doubly-connected domain shown in Fig. 5; it has been first analyzed in [5].

By setting $M_{\text{lim}} = 10000$, the best approximation corresponds to $m = 166$ and $q = 2$, with $M = 9960$ and the continuity error $e = 5.161e - 07$. The relevant warping function is evaluated by Eqs. (74 and 75) and is shown in Fig. 6.

The limit value $M = 9960$ corresponds to a very accurate solution, but it has required a computational time exceeding two hours. Table 1 shows the results of analyses relative to increasing values of M, along with the optimal values of m and q detected by means of Algorithm 6; the relevant values of the continuity error and the computational time are also reported.

It is worth noting that t refers to the total time required to perform Algorithm 6, so that more and more pairs (m, q) are explored as M increases and an increasing number of analyses need to be completed.

Please notice from Table 1 that when M is low enough the optimal solution corresponds to an increasing degree of the interpolating polynomials; conversely, as the total number of parameters increases the best solution corresponds to a finer discretization and linear interpolating functions.

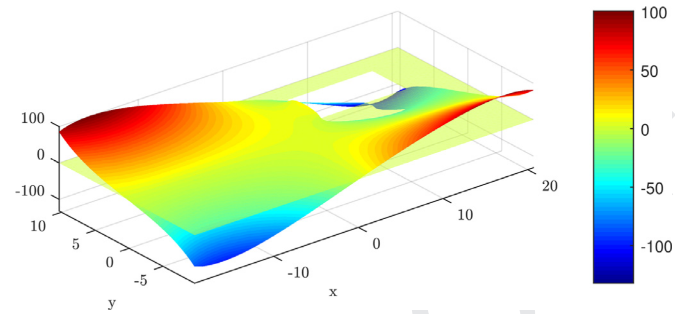

Fig. 6. Torsional warping function φ for to the doubly-connected domain in Fig. 5.

Table 1
Optimal values of m and q compatible with the fixed values of the total number of parameters M, along with the continuity error e and the computational time t, for the field φ of the doubly-connected domain in Fig. 5.

M	m	q	e	t [s]
60	1	2	4.914e-03	1.74e-01
150	1	5	6.350e-04	6.88e-01
300	2	5	1.974e-04	4.92e+00
600	5	4	5.936e-05	2.50e+01
1200	20	2	1.828e-05	1.45e+02
2460	41	2	5.393e-06	4.61e+02
4980	83	2	1.647e-06	2.34e+03
9960	166	2	5.161e-07	8.45e+03

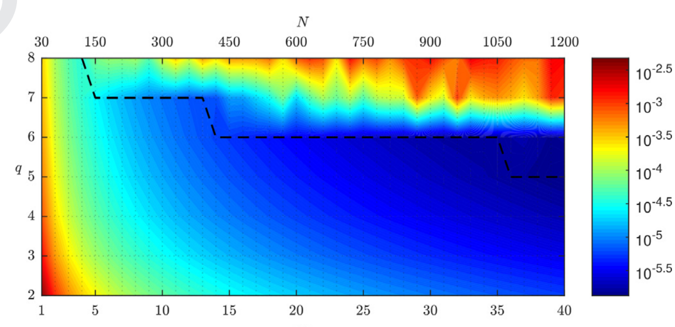

Fig. 7. Continuity error for φ with stability border (- - -) relevant to the doubly-connected domain in Fig. 5.

Such a feature is in line with the results of Fig. 7, in which the continuity error e is shown as function of the numerical parameters m and q. In particular, the trend of the limit of stability reveals how the maximum value of q providing reliable results decreases as the number of boundary elements increases.

6.4. Thin-walled domain

The analysis of the domain reported in Fig. 8, representing a bridge cross section, provides another example of results governed by the limit $M_{\text{lim}} = 10000$ rather than by the convergence of the continuity error.

Again the solution corresponding to the limit value $M = 9804$ is very accurate but it is very expensive in terms of computational time. The optimal parameters (m, q) and the relevant continuity error e for the scalar field φ are shown in Table 2 for increasing values of M, along with the required computational time.

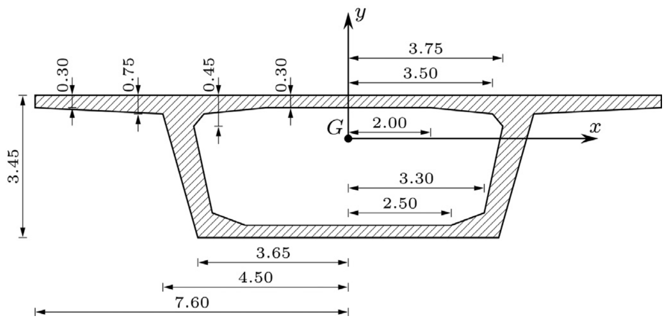

Fig. 8. Thin-walled domain.

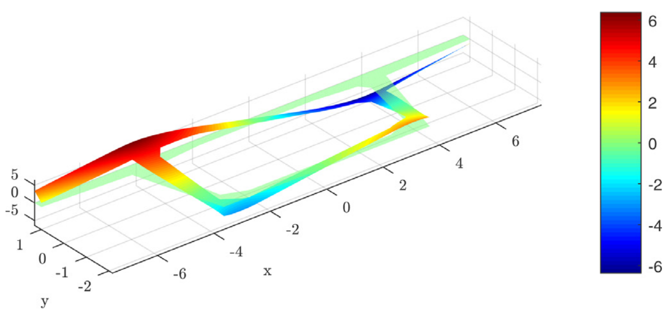

(a) Warping function φ.

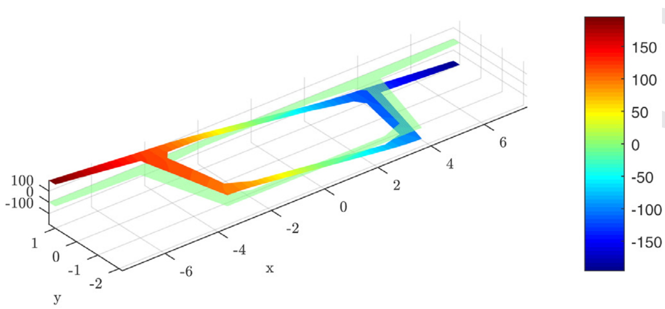

(b) Warping function ψ_x.

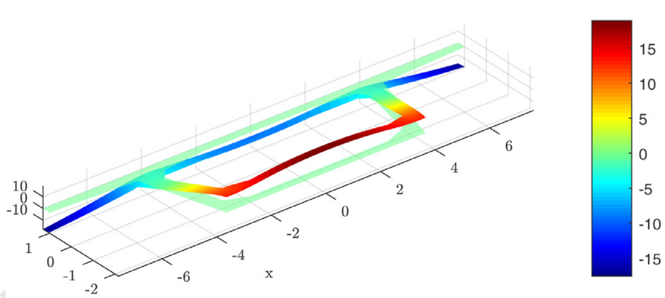

(c) Warping function ψ_y.

Fig. 9. Warping functions φ, ψ_x and ψ_y for the thin-walled domain in Fig. 8 ($\nu = 0.3$).

The analysis has been also conducted for the vector field $\boldsymbol{\psi}$, defined by the Neumann problems (1) and (2), respectively. The solution is expressed in terms of the scalar components ψ_x and ψ_y, explicitly considered in Section 4.2, and the values 0.0, 0.2 and 0.3 have been assigned to the Poisson ratio ν.

For all the scalar functions the best solution is found for $m = 18$ and $q = 3$, corresponding to $M = 9804$, with the continuity errors reported in Table 3. The functions φ, ψ_x and ψ_y, with reference to the case $\nu = 0.3$, are shown in Fig. 9.

Table 2
Optimal values of m and q compatible with the fixed values of the total number of parameters M, along with the continuity error e and the computational time t, for the field φ of the thin-walled domain in Fig. 8.

M	m	q	e	t [s]
382	1	2	4.757e-4	1.70e+0
573	1	3	2.016e-4	4.17e+0
1146	1	6	5.044e-5	4.35e+1
2204	3	4	1.600e-5	2.96e+2
4911	9	3	4.083e-6	1.66e+3
9804	18	3	1.183e-6	8.46e+3

Table 3
Continuity error e associated with $M = 9804$ for the thin-walled domain in Fig. 8.

ν	$e(\varphi)$	$e(\psi_x)$	$e(\psi_y)$
0.0		3.691e-06	1.251e-06
0.2	1.183e-06	3.679e-06	1.242e-06
0.3		3.674e-06	1.239e-06

7. Conclusions

A boundary element approach has been illustrated for a pure Neumann problem defined over an arbitrarily shaped polygonal domain. It has been addressed to evaluate the warping functions associated with torsion and shear in Saint Venant theory and in a recently derived beam model consistent with it [3]. A polynomial approximation of the unknown function has been assumed and, with the aim of optimizing the polynomial fitting, the Chebyshev nodes have been used as collocation points.

The choice of the Chebyshev nodes has also allowed us to exploit the elements' extremities, excluded from the set of collocation nodes, as points where one can evaluate the error in the continuity of the interpolating functions, a parameter assumed to be related to the accuracy of the numerical solution.

Actually, by partitioning the domain boundary as uniformly as possible, two parameters control the accuracy of the numerical solution, i.e. the number of elements relevant to the minimum length edge and the number of coefficients defining the polynomial function over each element. Expressing the continuity error as a function of such numerical parameters and imposing to be lower than a fixed tolerance, the discretization of the domain boundary and the degree of the interpolating polynomials can be conveniently set.

The numerical tests and the overall accordance with the results provided by the specialized literature [1,5] confirm the validity of the proposed approach, which also has the specificity of considering a proper parameter controlling the accuracy of the numerical solution.

In addition, numerical results have shown how, depending on the shape of domain, an improvement in the accuracy can be achieved by different approaches. In particular, compact domains do not require a very fine boundary discretization and the accuracy can be improved by increasing the degree of the interpolating polynomials. On the other hand, thin-walled domains show an instability in the method for high value of polynomial degree; hence, in order to obtain a sufficiently accurate solution it is convenient to adopt a finer discretization with linear interpolating functions.

In forthcoming papers the numerical strategy developed in this paper will be applied to evaluate the tensors required to consistently derive beam models from Saint Venant solid model, according to the formulation presented in [3], and to generate 1D finite elements that exactly recover elastic energy and displacements of the beam axis predicted by the 3D Saint Venant model.

Declaration of Competing Interest

None.

Acknowledgment

Financial support from the Italian Ministry of Education, University and Research (MIUR) in the framework of the Project PRIN COAN 5.50.16.01 - code 2015JW9NJT - is gratefully acknowledged.

Supplementary material

Supplementary material associated with this article can be found, in the online version, at doi:10.1016/j.enganabound.2020.01.004.

References

[1] Love AEH. A treatise on the mathematical theory of elasticity. New York: Dover Publications; 1944.
[2] Sokolnikoff IS. Mathematical theory of elasticity. New York: McGraw-Hill; 1946.
[3] Paradiso M, Marmo F, Rosati L. Consistent derivation of a beam model from the saint Venant's solid model. Int J Solids Struct 2019;159:90–110.
[4] Serpieri R. On the equivalence of energetic and geometric shear factors based on saint venant flexure. J Elast 2014;116:115–60.
[5] Lacarbonara W, Paolone A. On solution strategies to saint-Venant problem. J Comput Appl Math 2007;206:473–97.
[6] Barretta R, Barretta A. Shear stresses in elastic beams: an intrinsic approach. Eur J Mech A Solids 2010;29:400–9.
[7] Di Paola M, Pirrotta A, Santoro R. De saint-Venant flexure-torsion problem handled by Line Element-less Method (LEM). Acta Mech 2011;217:101–18.
[8] Romano G, Barretta A, Barretta R. On torsion and shear of Saint-Venant beams. Eur J Mech A Solids 2012;35:47–60.
[9] Barretta R. On stress function in Saint-Venant beams. Meccanica 2013;48:1811–16.
[10] Serpieri R, Rosati L. A frame-Independent solution to Saint-Venant's flexure problem. J Elast 2014;116:161–87.
[11] Kuchta M, Mardal KA, Mortensen M. On the singular neumann problem in linear elasticity. Numerical Linear Algebra with Applications 2019;26.
[12] Romano G, Rosati L, Ferro G. Shear deformability of thin-walled beams with arbitrary cross sections. Int J Numer Methods Eng 1992;35:283–306.
[13] Gruttmann F, Wagner W. Shear correction factors in Timoshenko's beam theory for arbitrary shaped cross-sections. Comput Mech 2001;27:199–207.
[14] Petrolo AS, Casciaro R. 3D Beam element based on Saint Venànt's rod theory. Comput Struct 2004;82:2471–81.
[15] Gruttmann F, Sauer R, Wagner W. Shear stresses in prismatic beams with arbitrary cross-sections. Int J Numer Methods Eng 1999;45:865–89.
[16] Dutta Roy T, Wittek A, Miller K. Biomechanical modelling of normal pressure hydrocephalus. J Biomech 2008;41:2263–71.
[17] Støverud KH, Alnæs M, Langtangen HP, Haughton V, Mardal KA. Poro-elastic modeling of Syringomyelia - a systematic study of the effects of pia mater, central canal, median fissure, white and gray matter on pressure wave propagation and fluid movement within the cervical spinal cord. Comput Methods Biomech Biomed Eng 2016;19(6):686–98.
[18] Tobie G, Čadek OP, Sotin C. Solid tidal friction above a liquid water reservoir as the origin of the South Pole hotspot on Enceladus. Icarus 2008;196:642–52.
[19] Padture NP, Gell M, Jordan EH. Thermal barrier coatings for gas-turbine engine applications. Science 2002;296:280–4.
[20] Zhang Y, Gu Y, Chen J-T. Boundary element analysis of the thermal behaviour in thin-coated cutting tools. Eng Anal Boundary Elem 2010;34:775–84.
[21] Muskhelishvili IN. Some Basic Problems of the Mathematical Theory of Elasticity. Groningen: Noordhoff; 1953.
[22] Hromadka II TV, Guymon GL. Complex polynomial approximation of the laplace equation. J Hydraul Eng 1984;110:329–39.
[23] Poler AC, Bohannon AW, Schowalter SJ, Hromadka II TV. Using the complex polynomial method with mathematica to model problems involving the laplace and poisson equations. Numer Methods Partial Differ Equations 2009;25:657–67.
[24] Hromadka II TV, Whitley RJ. Advances in the Complex Variable Boundary Element Method. London: Springer-Verlag; 1998.
[25] Whitley RJ, Hromadka II TV. Theoretical developments in the complex variable boundary element method. Eng Anal Boundary Elem 2006;30:1020–4.
[26] Lee JW, Hong HK, Chen JT. Generalized complex variable boundary integral equation for stress fields and torsional rigidity in torsion problems. Eng Anal Bound Elem 2015;54:86–96.
[27] Di Paola M, Pirrotta A, Santoro R. Line element-less method (LEM) for beam torsion solution (truly no-mesh method). Acta Mech 2008;195:349–64.
[28] Santoro R. The line element-less method analysis of orthotropic beam for the De Saint Venant torsion problem. Int J Mech Sci 2010;27:43–55.
[29] Bochev PB, Lehoucq RB. On the finite element solution of the pure neumann problem. SIAM Rev 2002;47:50–66.
[30] Steigemann M, Fulland M. On the computation of the pure Neumann problem in 2-dimensional elasticity. Int J Fract 2007;146:265–77.
[31] Dai X. Finite element approximation of the pure Neumann problem using the iterative penalty method. Appl Math Comput 2007;186:1367–73.
[32] Friedman Z, Kosmatka JB. Torsion and flexure of a prismatic isotropic beam using the boundary element method. Comput Struct 2000;74:479–94.
[33] Sapountzakis EJ, Mokos VG. Warping shear stresses in nonuniform torsion by BEM. Comput Mech 2003;30:131–42.
[34] Sapountzakis EJ, Mokos VG. A BEM solution to transverse shear loading of beams. Comput Mech 2005;36:384–97.
[35] Barone G, Pirrotta A, Santoro R. Comparison among three boundary element methods for torsion problems: CPM, CVBEM, LEM. Eng Anal Boundary Elem 2011;35:895–907.
[36] Cheng AH-D, Cheng DT. Heritage and early history of the boundary element method. Eng Anal Boundary Elem 2005;29:268–302.
[37] Gaspari D, Aristodemo M. Torsion and flexure analysis of orthotropic beams by a boundary element model. Eng Anal Boundary Elem 2005;27:850–8.
[38] Dikaros IC, Sapountzakis EJ. Nonuniform shear warping effect in the analysis of composite beams by BEM. Eng Struct 2014;76:215–34.
[39] Denda M, Dong FY. A unified formulation and error estimation measure for the direct and the indirect boundary element methods in elasticity. Eng Anal Boundary Elem 2001;25:557–64.
[40] Sladek V, Sladek J, Tanaka M. Regularization of hypersingular and nearly singular integrals in the potential theory and elasticity. Int J Numer Methods Eng 1993;36:1609–28.
[41] Ma H, Kamiya N. Distance transformation for the numerical evaluation of near singular boundary integrals with various kernels in boundary element method. Eng Anal Boundary Elem 2002;26:329–39.
[42] Xie G, Zhang J, Qin X, Li G. New variable transformations for evaluating nearly singular integrals in 2D boundary element method. Eng Anal Boundary Elem 2011;35:811–17.
[43] Hayami K, Matsumoto H. A numerical quadrature for nearly singular boundary element integrals. Eng Anal Boundary Elem 1994;13:143–54.
[44] Hayami K. Variable transformations for nearly singular integrals in the boundary element method. Publ Res Inst Math Sci 2005;41:821–42.
[45] Gao X-W, Yang K, Wang J. An adaptive element subdivision technique for evaluation of various 2D singular boundary integrals. Eng Anal Boundary Elem 2008;32:692–6.
[46] Gao X-W. Numerical evaluation of two-dimensional singular boundary integrals–theory and fortran code. J Comput Appl Math 2006;188:44–64.
[47] Padhi G, Shenoi R, Moy S, McCarthy M. Analytic integration of kernel shape function product integrals in the boundary element method. Comput Struct 2001;79:1325–33.
[48] Zhou H, Niu Z, Cheng C, Guan Z. Analytical integral algorithm applied to boundary layer effect and thin body effect in BEM for anisotropic potential problems. Comput Struct 2008;86:1656–71.
[49] Niu Z, Cheng C, Zhou H, Hu Z. Analytic formulations for calculating nearly singular integrals in two-dimensional BEM. Eng Anal Boundary Elem 2007;31:949–64.
[50] Chen H, Lu P, Schnack E. Regularized algorithms for the calculation of values on and near boundaries in 2D elastic BEM. Eng Anal Boundary Elem 2001;25:851–76.
[51] Johnston PR, Elliott D. A sinh transformation for evaluating nearly singular boundary element integrals. Int J Numer Methods Eng 2005;62:564–78.
[52] Johnston PR, Johnston BM, Elliott D. Using the iterated sinh transformation to evaluate two dimensional nearly singular boundary element integrals. Eng Anal Boundary Elem 2013;37:708–18.
[53] Xie G, Zhang J, Dong Y, Huang C, Li G. An improved exponential transformation for nearly singular boundary element integrals in elasticity problems. Int J Solids Struct 2014;51:1322–9.
[54] Zieniuk E. Potential problems with polygonal boundaries by a BEM with parametric linear functions. Eng Anal Boundary Elem 2001;25:185–90.
[55] Chen JT, Lin SR, Chen KH. Degenerate scale problem when solving Laplace's equation by BEM and its treatment. Int J Numer Methods Eng 2005;62:233–61.
[56] Chen JT, Huang WS, Lee YT, Kuo SR, Kao SK. Revisit of degenerate scales in the BIEM/BEM for 2D elasticity problems. Mech Adv Mater Struct 2015. doi:10.1080/15376494.2015.1091526.
[57] Li ZC, Zhang LP, Lee MG. Interior field methods for Neumann problems of Laplace's equation in elliptic domains, comparisons with degenerate scales. Eng Anal Bound Elem 2016;71:190–202.
[58] Corfdir A, Bonnet G. Degenerate scale for 2D Laplace equation with Robin boundary condition. Eng Anal Boundary Elem 2017;80:49–57.
[59] Yoon M, Yoon G, Min C. On solving the singular system arisen from Poisson equation with Neumann boundary condition. J Sci Comput 2016;69:391–405.
[60] Katsikadelis JT. Boundary Elements: Theory and Applications. Amsterdam: Elsevier Science; 2002.
[61] Lutz E, Ye W, Mukherjee S. Elimination of rigid body modes from discretized boundary integral equations. Int J Solids Struct 1998;35:4427–36.
[62] Paradiso M., Vaiana N., Sessa S., Marmo F., Rosati L.. A BEM approach to the evaluation of warping functios in the Saint Venant theory - Supplementary material. 2019b. https://app.box.com/s/tlatc79fk7b7qh1oonakzqyqhyyienxu (accessed Dec. 2019). Q2